El Chichón Volcano: Eruptive History

3

Teresa Scolamacchia and Lucia Capra

Abstract

El Chichón volcano became known worldwide after it erupted catastrophically in 1982 and killed an estimated 2,000 people. A cumulative mass of almost 8 million tons of sulfur dioxide was injected into the stratosphere. The first reconstruction(s) of the stratigraphic successions carried out at the volcano shortly after the eruption suggested a long record of eruptive activity in the geologic past. Many studies completed in the past decade, aided by $^{40}Ar/^{39}Ar$ and K/Ar dating, have confirmed that the eruptive activity indeed was long lasting, occurring from eruptive centers located several km apart, before migrating at its present position. Within this context, El Chichón might better be described as a Volcanic Complex rather than a single volcano. During the Holocene at least 12 explosive eruptions originated from the same vent that was reactivated in 1982 producing pyroclastic density currents (PDCs) along many of the same pathways as those in 1982. This chapter summarizes the spatial and temporal evolution of this volcanic complex, integrating some previously unpublished data with the existing information. The time sequence of the 1982 eruptive events has been re-examined considering records from far-away stations and eyewitnesses' accounts that were not taken into account in previous studies, providing a more coherent time-stratigraphic framework for the 1982 eruptive sequence. Considering El Chichon's history of past eruptions, the existence of a wide, shallow, groundwater table and the re-establishment of an active hydrothermal system after the 1982 eruption, the probability of a new phreatic/phreatomagmatic eruption may still exist.

3.1 Previous Works

El Chichón was recognized as an active volcano in the early 20th century by Müllerried (1932, 1933), who visited the area following a period of seismic unrest at a small hill known as Cerro la Unión (Fig. 3.1). He reported the presence of stalactites of native sulfur near fumaroles discharging H_2S, and hot springs between a 1,260 m high dome and a major crater structure, which later would be recognized as the Somma crater.

T. Scolamacchia (✉)
Department of Earth and Environmental Sciences, LMU, Theresienstrasse 41, Munich, 80333, Germany
e-mail: tscolamacchia@gmail.com

L. Capra
Campus UNAM Juriquilla, Centro de Geociencias, Boulevard Juriquilla, no. 3001, Juriquilla, Queretaro 76230, Mexico

T. Scolamacchia and J.L. Macías (eds.), *Active Volcanoes of Chiapas (Mexico): El Chichón and Tacaná*, Active Volcanoes of the World, DOI 10.1007/978-3-642-25890-9_3,

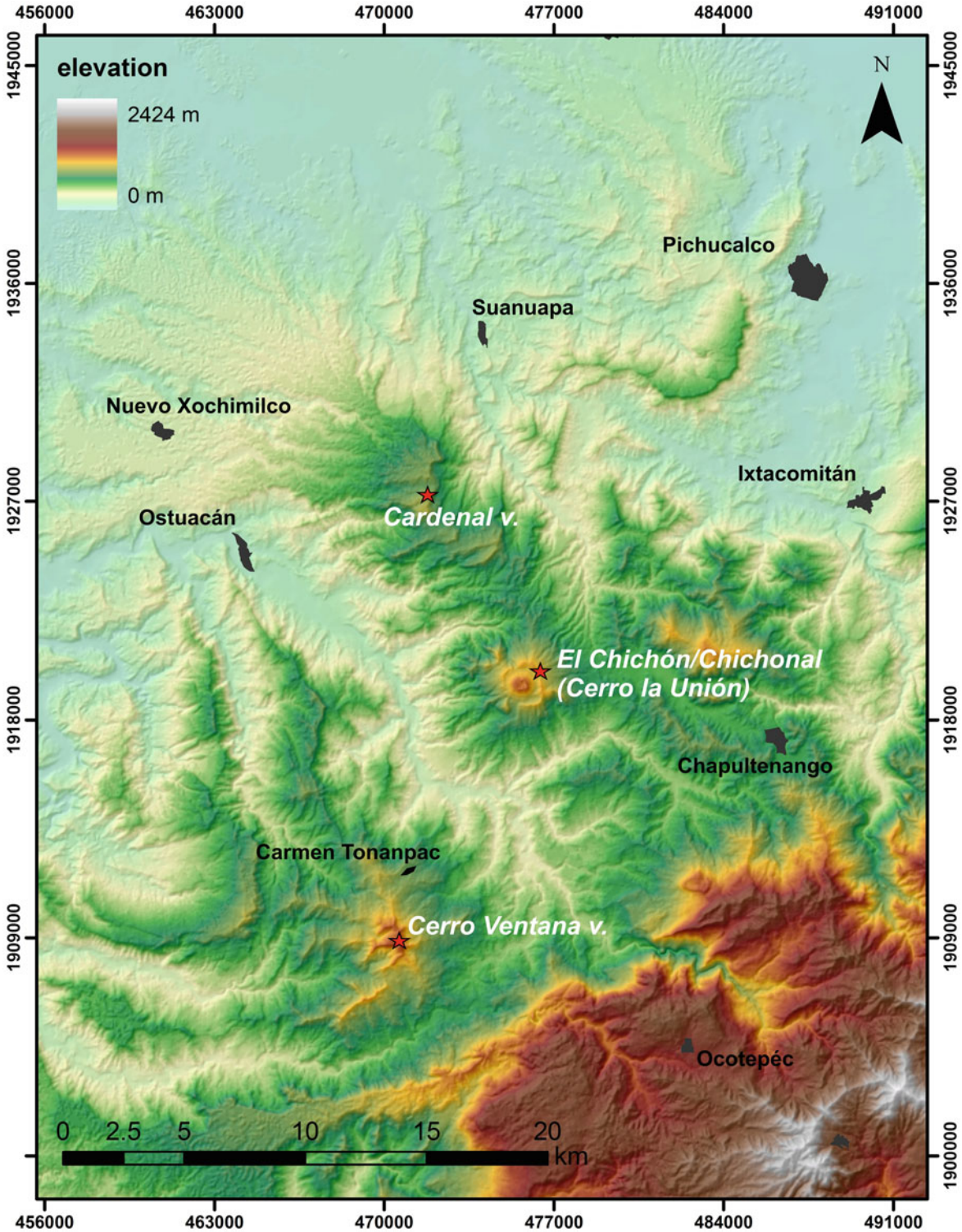

Fig. 3.1 Digital elevation model of El Chichón volcano (also known as Chichonal or La Unión) and surrounding areas illustrating the locations of other now-dormant volcanic structures (e.g. Catedral volcano and Cerro Ventana volcano) and the regional morphology controlled by the main folds and faults in the area

After this early study, El Chichón was included in the list of active volcanoes of the world of the International Association of Volcanology and Chemistry of the Earth's Interior (IAVCEI) (Mooser et al. 1958).

Further studies were carried out only 50 years later by Damon and Montesinos (1978), who were searching for ore deposits, and were the first to obtain K-Ar ages of 209 ± 19 ka for rocks that crops out in the eastern sector of the volcanic edifice (Somma crater). Following their work, Mexico's National Power Company—Comisión Federal de Electricidad (CFE)—began the evaluation of the area for its geothermal energy exploitation. During these studies, which produced the first geological map of the volcano (Canul and Rocha 1981), Templos et al. (1981) reported the presence of thermal waters on the southern flanks of the volcano. Canul and Rocha (1981) described fumarolic activity and altered ground around the central dome, and along a fault cutting the dome, warning about a potential volcanic risk in the area, after being witnesses of earthquakes and rumbling sounds when doing fieldwork. Unfortunately, both reports remained unpublished and were not taken into account, thereby contributing to the disastrous outcome of the 1982 eruption (see Chap. 8).

The 1982 catastrophic eruption motivated the research in the area to determine the eruptive history of the volcano. The dense tropical vegetation cover around the volcano had been stripped by the eruption, allowing excellent exposures of the pre-1982 deposits.

A first reconstruction of the eruptive history of the volcano was provided by Canul et al. (1983), however, these authors did not present any age constraints for the eruptive deposits. Several studies followed aimed at reconstructing the stratigraphic succession of the 1982 eruption (e.g. Sigurdsson et al. 1984, 1987; Carey and Sigurdsson 1986) and its past eruptive history. Duffield et al. (1984) defined the volcano as a "tuff cone surrounded by a ring of domes". The use of the term "tuff cone", a volcanic landform typically associated to the emplacement of pyroclastic sequences related to hydromagmatic activity involving abundant quantities of water (Wohletz and Sheridan 1983), suggests that the abundance of deposits from such kind of activity was already recognized in this early study. Rose et al. (1984) mapped the newly formed crater, and recognized several fault trends within the crater floor, defining El Chichón as a "complex of domes emplaced around a ring fracture". Tilling et al. (1984) provided the first reconstruction of the eruptive activity during the Holocene. Further works in the 1990s allowed to refine the 1982 stratigraphic succession, and recognized the presence of older structures (Macías 1994; Macías et al. 1997, 1998).

The intense erosion in the region, due to the very high (>4,000 mm) average annual rainfall (Atlas del Agua 1976), created deep gullies following 1982, exposing older deposits around the volcano. This situation favored detailed stratigraphic studies of the Holocene deposits (Espíndola et al. 2000). This work inspired other studies in the following 10 years, aimed either at refining the 1982 and previous stratigraphic successions, or to understand better how the structural setting of the region influenced the volcanic activity (Macías et al. 2003, 2004, 2008; García-Palomo et al. 2004; Scolamacchia and Macías 2005; Scolamacchia et al. 2005; Sulpizio et al. 2008; Scolamacchia and Schouwenars 2009).

A more complete scenario of the temporal evolution of El Chichón's eruptive history, including pre-Holocene activity, was obtained recently (Layer et al. 2009; Macías et al. 2010) combining photo geological interpretation, stratigraphic records, and K–Ar and C^{14} ages from previous works, with new ^{40}Ar-^{39}Ar ages and structural studies. All these studies evidenced the presence of several volcanic structures, mostly domes and ancient craters, which were emplaced along major faults oriented E-W and NNW–SSE (see Chap. 1). For these reasons, El Chichón has been recently defined a volcanic complex (Layer et al. 2009; Macías et al. 2010).

Very recent interpretations of ground-based geomagnetic and aeromagnetic surveys (Juetzler et al. 2011) made possible the characterization of underground magnetic bodies and hydrothermal vents and to relate them in comparison with results from previous studies.

The following sections summarize the spatial and temporal evolution of the El Chichón Volcanic Complex, combining the data reported in previous work, and proposing a different interpretation of some events for which discrepancy exists in the literature.

Inset Box: Nomenclature Used

The eruptive history of El Chichón has been characterized by the occurrence of explosive eruptive events. It is therefore important to clarify the terms that are used in this chapter to refer to the products of such activity.

Pyroclastic density currents (PDCs, Fisher 1990) are multiphase flows of gases and volcanic fragments that flow under the influence of gravity, which may originate in different ways (Branney and Kokelaar 2002). Considering that different types of PDCs produce similar depositional facies (Branney and Kokelaar 2002), the simple observation of deposits, give convoluted data from which to infer eruptive mechanisms. For this reason, sedimentological analyses, and the observation of the morphology of juvenile particles are often necessary. Early works classified PDCs deposits based on their lithology and sedimentary structures, into pumice and ash flows (ignimbrites), block and ash flows, and pyroclastic surges (e.g. Fisher and Schmincke 1984; Cas and Wright 1987). The currents produced by explosive hydromagmatic activity were named "base surges" (Richards 1959; Moore et al. 1966; Moore 1967; Fisher and Waters 1970; Waters and Fisher 1971) due to their similarity with the ones produced in nuclear explosions, observed moving radially at the base of a collapsing low-altitude column (Brinkley et al. 1950; Young 1965). Base surges (fully dilute pyroclastic density currents of Branney and Kokelaar 2002) are envisaged to have a lower solid concentration (≤0.1–1 vol%, Valentine and Fisher 2000), with respect to other currents (i.e. pyroclastic flows, ≥10 vol%, Freund and Bursik 1998).

The probability of occurrence of an explosive interaction between magma and external water, and the intensity of such interaction, is determined by mixing conditions. Experiments with silicate melts (Zimanowski et al. 1997a, b; Büttner and Zimanowski 1998), and others studies (e.g. Colgate and Sigurgeisson 1973; Kokelaar 1986), indicated that the probability is higher when water gets entrapped into magma. Under such confined conditions, the heat transfer between magma and water is limited by the formation of a vapor film, which isolates the two media allowing the water to persist in a metastable state. The collapse of the film (i.e. due a seismic wave) causes the direct contact between the two media enhancing the heat transfer rate (up to 10^6 K/s, Zimanowski 1998; Zimanowski and Wohletz 2000), and causing a very fine fragmentation of the melt. For this reason the particles produced by this high energetic process typically have very small grain sizes (32 μm < d < 130 μm), and represent a small fraction (e.g. 5–10 wt%) of the entire deposit, which consists mostly of fragmented country rocks (Sheridan and Wohletz 1983a; Zimanowski and Wohletz 2000). The particles produced by this interaction show a distinctive morphology (i.e. *blocky shapes* of Heiken and Wohletz 1985), attesting the occurrence of a brittle fragmentation.

The amount of water entering in contact with magma (e.g. Heiken 1971; Wohletz and Sheridan 1979; Sheridan and Wohletz 1981, 1983a; Wohletz 1983; Kokelaar 1986; Zimanowski et al. 1997a), and the critical interface between the two media (Zimanowski et al. 1997a, b; Büttner and Zimanowski 1998; Austin-Ericksson et al. 2008), represent critical factors for the occurrence of an explosive interaction. For values close to an optimum water/magma ratio (i.e. 1:10 in volume Zimanowski and Wohletz 2000), all the water involved in the process is converted into superheated steam, producing mixtures with temperatures ≥100 °C (i.e. "dry" pyroclastic surges) while, for water values exceeding the optimum ratio, the water is not completely vaporized, and remains as liquid droplets inside the clouds, producing "wet" pyroclastic surges (Moore 1967; Waters and Fisher 1971; Wohletz and Sheridan 1979; Sheridan and Wohletz 1981; Wohletz and Sheridan 1983). Experiments using different water/magma mass ratios to reproduce the conditions existing during "dry" and "wet" hydromagmatic eruptions, have shown the efficiency of the interaction is the same (Büttner et al. 1999).

The structural and textural characters of "wet" surge deposits, such as the irregular contacts between beds produced by the load of damp deposits on others still plastic beneath, the presence of vesicles and aggregates, the plastering against overhanging surfaces, the abundant content of fine ash, the poor sorting, and the rapid hardening of the deposits (Waters and Fisher 1971; Lorenz 1974; Wohletz and Sheridan 1983) would reflect the influence of condensing water

vapor on the depositional mechanisms of such PDCs. Such characters are absent in "dry" surge deposits, which are generally coarser in grain-size, with minor amounts of medium to fine ash, better sorted, and display variable structures evidencing a transporting medium rich in superheated steam (Walker 1971; Sheridan and Wohletz 1983a; Wohletz 1983).

3.2 Eruptive History

3.2.1 Pre-holocene Activity

The oldest evidence of volcanism in the area is represented by a dissected crater structure located ~4 km NW of the present crater on the trace of a major fault that runs NNW–SSE (Chichón-Catedral fault, see Chap. 1). Recent studies (Macías et al. 2010) indicated that this crater would represent a portion of a former volcanic edifice (Catedral volcano) collapsed toward the SE (Fig. 3.1). Undifferentiated pyroclastic products related to the activity of this ancestral edifice have been recognized to the NW. $^{40}Ar/^{39}Ar$ data on lithic blocks embedded in such deposits, yielded ages of 1.64 Ma (Chap. 1), indicating that this structure could represent the oldest volcanic edifice in the area but further studies are needed in order to constrain this old period of activity.

The volcanism shifted then 14 km to the SW, with the emplacement of a trachybasaltic dike (46–49 wt% SiO_2) that crops out in the outskirts of Chapultenango village, 10 km E from the actual crater. The emplacement of this dike, dated at 1.1 Ma (K–Ar), occurred along the eastern tip of the E–W strike slip San Juan fault, which runs across the volcanic complex (García-Palomo et al. 2004).

The onset of the construction of El Chichón's volcanic edifice at its present location, is inferred to have occurred in the Middle Pleistocene, based on a $^{40}Ar/^{39}Ar$ age of 372 ± 5 ka obtained on a lithic block collected inside 1982 pyroclastic products (Layer et al. 2009). Nevertheless, no other field evidences have been found on the early stages of the edification of the Somma (*Pre-Somma* of Layer et al. 2009) until the present (Fig. 3.2a).

3.2.1.1 Edification of Somma (276–55 Ka)

The Somma edifice with a maximum elevation of 1,150 m a.s.l., is a 1.5 × 2 km wide crater. It consists of annular steep dome extrusions of porphyritic trachyandesites (**Unit O** of Espíndola et al. 2000) surrounded by aprons of indurated deposits of trachyandesitic blocks immersed in a matrix of lapilli and ash, exposed as far as 2.5 km W (**Unit N** of Espíndola et al. 2000; **Unit E** of Tilling et al. 1984) interbedded with volcaniclastic deposits (Layer et al. 2009). These deposits are widely distributed around the volcano and significantly determine its morphology (Fig. 3.2a). The Somma edifice occupies an area of 40 km^2, with an estimated volume of 18 km^3 (Layer et al. 2009). Trachyandesitic dome rocks (57.8 wt% SiO_2) collected on the eastern rim of the Somma crater yielded K–Ar ages between 276 ± 6 ka (Duffield et al. 1984) and 209 ± 19 ka (Damon and Montesinos 1978), which would indicate that dome extrusion occurred in a lapse of time of approximately 77 ka (Layer et al. 2009). This activity was accompanied by dome destruction with the generation of several pyroclastic density currents (PDCs) rich in non vesicular blocks (i.e. block and ash flows), as indicated by $^{40}Ar/^{39}Ar$ isochron ages of 55 ± 6 ka on blocks of porphyritic trachyandesites from these deposits collected on the W flank (Macias et al. 2010, Fig. 3.2a), and were subsequently remobilized as lahars (Layer et al. 2009).

A gray, porphyritic lava flow (58.99 wt% SiO_2) found 2 km to the NE flank of the Somma crater (**Unit M** of Espíndola et al. 2000), was probably related to a minor episode of effusion following domes emplacement in this sector, considering their similar composition. The lapse of time during which this lava flow was emplaced is not clear since the $^{40}Ar/^{39}Ar$ ages of 15 ± 7 ka obtained on lava flow samples show large standard deviation due to excess of Ar (Layer et al. 2009), and similar ages of 12 ± 6 ka, were also obtained for samples of dome remnants on the E-SE Somma rim (Layer et al. 2009). Apparently, a mayor eruption destroyed the central part of the Somma dome complex during Late Pleistocene and formed a 1.5 km wide crater (Fig. 3.2a). The type and magnitude of the eruption are still unknown (Layer et al. 2009).

3.2.1.2 Lateral Dome Extrusion (217–44 Ka)

Dome extrusion continued during the Middle and Upper Pleistocene on peripheral areas of the Somma

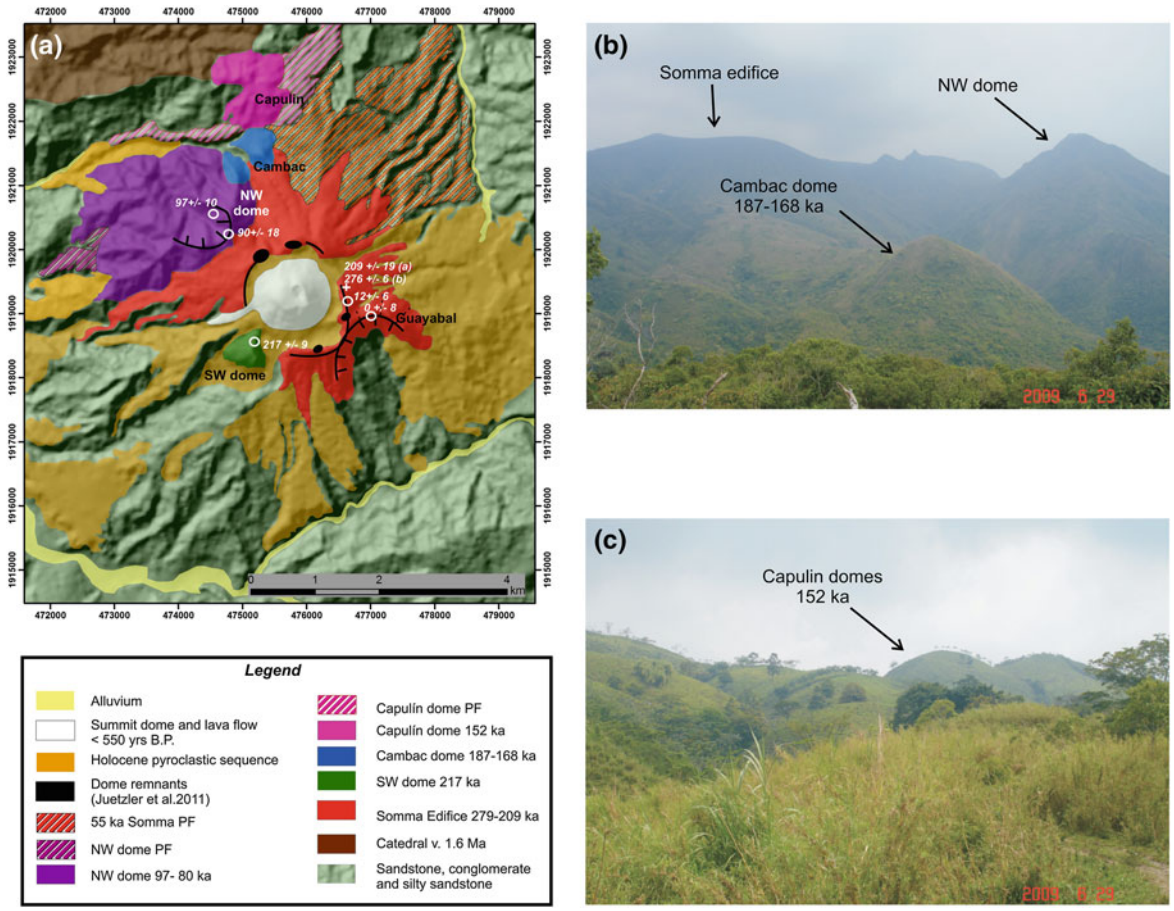

Fig. 3.2 **a** Digital elevation model showing the distribution of the folded/faulted sedimentary basement, and the structures and deposits of the different stages of the development of El Chichón Volcanic Complex. The lava dome extruded after the 550 years B.P. eruption represents the most recent constructive landform. Note the tree main notches that dissect the Somma crater to the E, N and SW. Samples dated by Layer et al. (2009) are indicated by *white circles*, while **a** and **b** indicated samples dated by Damon and Montesinos (1978) and Duffield et al. (1984), respectively; **b** panoramic view of the domes Cambac and NW, on the northern flanks of the volcano. **c** Photograph of the Capulin domes taken from the N (*Photo* by JL Arce)

edifice. To the SW, a weakly incised dome, with a maximum elevation of 900 m a.s.l. and 300 m high walls occupies an area of 0.32 km^2 with an approximate volume of 0.1 km^3 (Fig. 3.2a) (Layer et al. 2009). Canul and Rocha (1981) described for the first time this structure as "lateral dome". A sample of a massive, poorly altered trachyandesite (58.2 wt% SiO_2), collected from the dome summit yielded an $^{40}Ar/^{39}Ar$ age of 217 ± 9 ka.

Duffield et al. (1984) proposed that the SW dome was associated with a 1.2 km wide crater. Nevertheless, no evidence of deposits associated to this activity exists. According to Layer et al. (2009), the extrusion of the SW dome determined a partial disruption of part of the southwestern rim of the Somma crater, forming a 1.2 km wide collapse scar. This interpretation agrees with recent data presented by Jutzeler et al. (2011). The disruption of the southwestern Somma rim would indicate that dome extrusion occurred sometime after or was contemporaneous with the formation of the Somma crater (Layer et al. 2009). Alternatively, the scarp around the SW dome could be a feature formed by the differential erosion around the dome in contact with the rocks of the sedimentary basement. Such rocks crop out in the coalescing escarpments of the Tuspac river. This interpretation would be supported by the similar morphology of the Somma crater to the NE, discontinuous as the one to the SW.

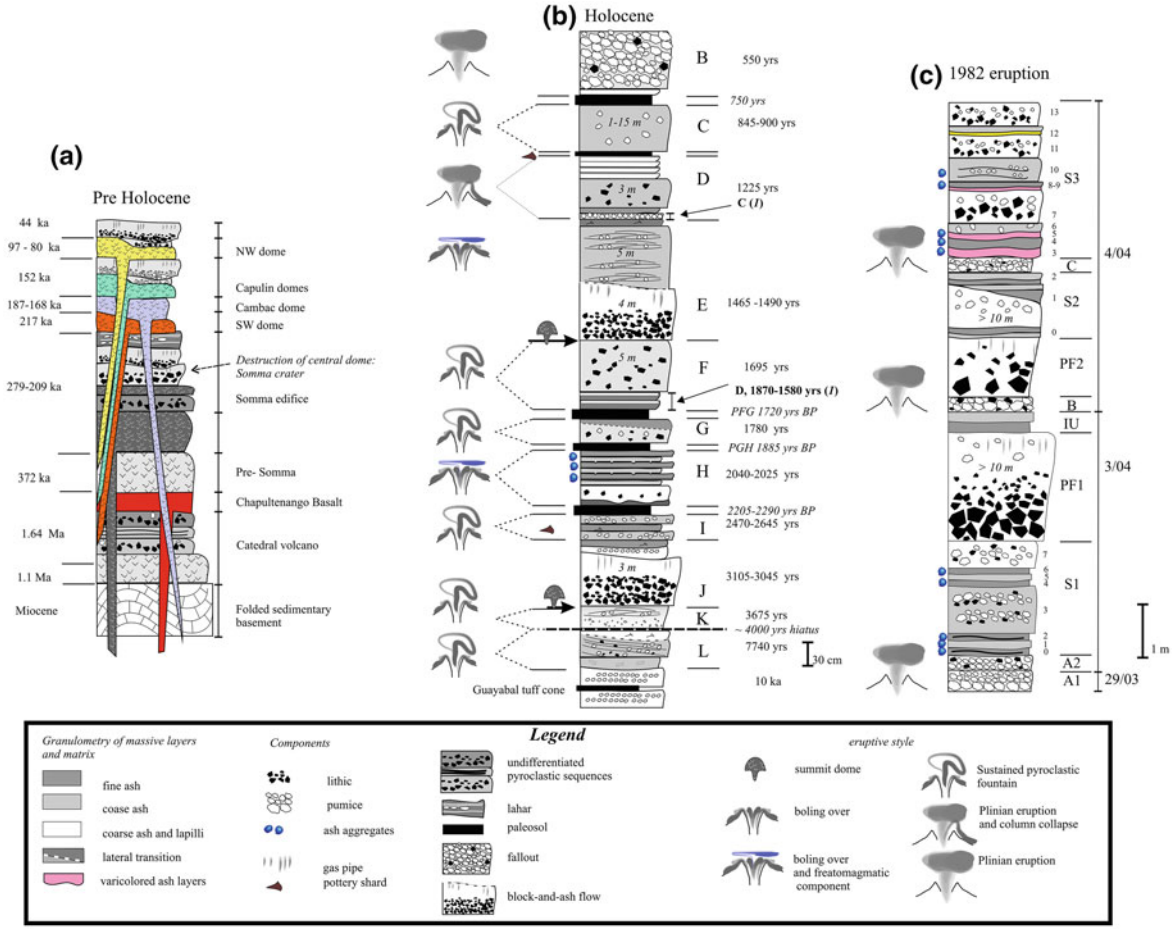

Fig. 3.3 Composite stratigraphic sections illustrating the eruptive history of El Chichón Volcanic Complex. **a** Pre-holocene stratigraphy. **b** Holocene stratigraphy showing the inferred eruptive episodes based on studies by Tilling et al. (1984) and Espíndola et al. (2000). The interpretation presented in this work about the eruptive style is also shown. **c** Stratigraphic composite section of the 1982 eruption, the timing of different phases is based on this work, see text for more detail. (1) Unit name according to Tilling et al. (1984) Table 3.1 and Fig. 3.2

Other two low-altitude (720 m a.s.l.) domes of porphyritic trachyandesites (56 wt% SiO_2) were extruded on the NW flanks of the Somma between 187 ± 13 and 168 ± 37 ka (Fig. 3.2a, b) according to $^{40}Ar/^{39}Ar$ isochron ages (Cambac domes, Macías et al. 2010). The trachyandesites from these domes contain biotite crystals beside a common association of plagioclase, amphiboles, and clinopyroxenes phenocrysts immersed in a glassy matrix (see Chap. 2).

Dome extrusion continued ~3 km NNE of the present crater, around 152 ± 21 ka, emplacing other 6 domes alineated in an E–W direction (Capulin domes, Macías et al. 2010). These domes consist of porphyritic trachyandesites (57.8 wt% SiO_2), with a maximum height of 740 m a.s.l. (Figs. 3.2a–c, and 3.3a).

Dome extrusion was apparently followed by their explosive destruction, as attested by the presence of block and ash flow deposits, consisting of trachyandesitic blocks (56 wt% SiO_2), with a common association of plagioclase, hornblende, clinopyroxenes phenocrysts in a glassy matrix, immersed in coarse ash, which reached distances of 3 km to NE and to the SW. Blocks from these deposits yielded $^{40}Ar/^{39}Ar$ ages between 102 ± 7 ka (to the NE) and 48 ± 3 ka (to the SW). The activity of dome destruction probably continued until 44 ± 10 ka as indicated by $^{40}Ar/^{39}Ar$ isochron ages on accidental lithics found in the 1982 deposits.

As the explosive destruction of Capulin domes was taking place, another dome was extruded to the NW

flank of the Somma. The 1,048 m a.s.l. NW dome (Macías 1994; Macías et al. 1997), is a highly eroded structure characterized by a deep drainage, and consists of gray to green partially altered porphyritic basaltic trachyandesitic lavas (55.84–56.28 wt% SiO_2). It occupies an area of ≈5 km^2, with an estimated volume of 3 km^3 (Layer et al. 2009). A 700 m wide collapse structure left a horseshoe shaped crater opened to the NW. Dome samples used to date this episode gave $^{40}Ar/^{39}Ar$ isochron ages ranging between 97 ± 10 ka (Layer et al. 2009) and 80 ± 23 ka (Macias et al. 2010).

Recent results of high-resolution ground-based geomagnetic and aeromagnetic surveys (Jutzeler et al. 2011) evidenced strong magnetic anomalies (TMI) around the Somma rim and inside the 1982 crater. The largest TMI anomalies are located in correspondence to the NW and SW domes, and on the E–SE rim of the crater Somma, corresponding to dome remnants dated by Layer et al. (2009) at 12 ± 6 ka (Figs. 3.2a, and 3.3a).

These highly magnetized bodies, which would extend at depths between <200 m (for the E–SE rim and SW dome) up to 500 m (NW dome), were interpreted as cryptodomes in which only the uppermost part was extruded (Jutzeler et al. 2011). In this light, the large ridges and the topographic depressions formed around the NW dome would be related to sector collapse associated with the growth of cryptodomes (Fig. 3.2a). Alternatively, the collapse scar observed near the NW dome, could also have been caused by the movement of a major fault oriented NNW to SSE (Chichonal-Catedral fault) whose trace intersects the NW dome, as suggested recently by Macías et al. (2010).

3.2.1.3 Guayabal Tuff Cone (~10 Ka)

The next locus of activity migrated on the flanks of the Somma crater, 3 km to the SE of the Somma rim, determining the formation of the Guayabal "tuff cone" (Macías 1994).

The Guayabal cone is a 700 m wide horseshoe shaped crater, with a maximum elevation of 950 m a.s.l., opened to the SE into the Agua Caliente gully (Fig. 3.4) and in direct contact with porphyritic andesites of the Somma crater (Layer et al. 2009). A fault oriented NW-SE (Chichón-Catedral fault; Macias et al. 2010) runs inside Agua Caliente gully. The cone collapsed toward the SE leaving only a semicircular wall to the NE. This wall exposes a sequence of undifferentiated pyroclastic units, at least 3 m thick, separated by paleosols. No detailed descriptions are available for these pyroclastic deposits and they may refer to pyroclastic density currents (PDCs) produced by either hydromagmatic or magmatic activity. A massive to stratified deposit succession interpreted as the product of a hydromagmatic activity (i.e. pyroclastic surge), caps the entire depositional sequence and contains boulders of Cretaceous limestones from the volcano basement, which are also abundant in the andesites beneath (Espíndola et al. 2000). No useful age constrains exist to date the eruptive activity occurred from this center. In fact, $^{40}Ar/^{39}Ar$ dating of a porphyritic andesite from the dome rock forming the substrate of this cone yielded an imprecise age of 100 ± 600 ka, due to excess atmospheric argon. Moreover, a porphyritic andesite fragment embedded in the pyroclastic surge deposit that caps the sequence yielded a $^{40}Ar/^{39}Ar$ age of 0 ± 8 Ka.

Fig. 3.4 View from the SE of the remnants of the Guayabal cone. The *dashed white line* separates the base of the cone from the porphyritic andesites extruded on the Somma flanks. Note the 700 m wide horseshoe-shaped depression of Agua Caliente gully

Based on the overall appearance of the deposits, Layer et al. (2009) suggested that the type of activity that build up the Guayabal cone was mostly hydromagmatic in character. Nevertheless, the presence of paleosols separating pyroclastic sequences suggests that several explosive eruptions occurred from this eruptive center, even if more detailed studies would be useful to determine the type of eruptive events occurred.

3.2.2 Holocene Activity

The locus of volcanic activity during the Holocene returned again to the area of the Somma crater (Tilling et al. 1984; Espíndola et al. 2000; Layer et al. 2009).

Stratigraphic relationships and radiocarbon dating indicated that at least 11 explosive eruptions and domes extrusions occurred during the past 8,000 years (Fig. 3.3b; Espíndola et al. 2000). Radiocarbon dates reported here were calibrated with the program CALIB 5.0 (Stuiver and Reimer 1986); the sigma-1 range is reported in years calibrated before present (yr cal BP) and based on the calibration curve IntCal04 (Reimer et al. 2004). *Anno Domini* calibrated (AD cal) ages are also provided when needed. According to Espíndola et al. (2000), the best outcrops for Holocene deposits are located on the eastern and southern sides of the volcano at distances between 6 and 12 km from the present crater (Fig. 3.6).

The first record of activity in the Holocene was found in a ravine 4 km to the NW of the crater. It consists of a brown deposit (30 m thick) of coarse pumice and scarce andesitic lapilli immersed in a matrix of coarse ash, characterized by a diffuse stratification of the pumice lapilli, which is strongly erosive on a debris flow deposit of rounded blocks of limestone from the local basement immersed in a clayish matrix. This deposit transforms 4 m downstream into a massive deposit of coarse ash and lapilli. Embedded charcoal fragments yielded ^{14}C ages of 7740 ± 50 year BP (8454–8558 cal year BP) (**Unit L**, Espíndola et al. 2000). The textural and structural characters of the deposits, and the absence of an underlying fallout layer, suggest that this unit was probably emplaced by a sustained current produced by the prolonged collapse of a low-altitude column (i.e. "boiling over" activity of Taylor 1958). Apparently, no other activity occurred for approximately 4,000 years, or the deposits, if any, from minor activity, were eroded and not preserved. In fact, the following ^{14}C data of 3675 ± 80 year BP (3895–4094 cal year BP), refers to charcoal fragments embedded in an altered, brown deposit (12–220 cm thick) that crops out at distances of up 10 km in the eastern and southern sectors, between Chapultenango and C. Tonapac, above basement rocks and underlies a widespread yellow pumice fallout layer (unit B, see below). In the outskirts of G. Victoria village, 8 km SE from the crater, the deposit consists of a basal massive thick layer of coarse ash with subrounded andesitic lithic lapilli and scatter pumice lapilli, which gradually become more pumice-rich toward the top, with subrounded yellow pumice layers and lenses (**Unit K** of Espíndola et al. 2000, Fig. 3.3b). The deposits characteristics and their great areal extent, suggest that Unit K was emplaced by a sustained lateral current derived from the collapse of a tall eruptive column, during which pumice fallout fell into the current, and become rounded by collision/abrasion at the contact with other clasts, without being recorded as a pumice fall layer.

A dome apparently grew inside the central crater afterward and, after a period of ~600 years was explosively destroyed; probably hydromagmatic activity also occurred (Espíndola et al. 2000). Evidences for this eruptive activity are recorded by deposits that crop out at distances of 2.5 km to the E, inside El Platanar valley, and were attributed to the same period considering their similar radiocarbon age ranging between 3105 ± 70 year BP (3241–3397 cal year BP) and 3045 ± 105 year BP (3139–3371 cal year BP) (**Unit J**, Espíndola et al. 2000). They consist of a pink to gray massive, clast-supported deposit of andesitic lithic blocks immersed in a scarce matrix of lithic and pumice lapilli, with relict vertical fumarolic pipes at one side of the valley, and of a greenish to–gray deposit (3 m thick), of alternating beds of fine and coarse ash and massive beds of ash and lapilli containing tree casts, on the opposite side. The abundance of andesitic blocks in the deposit was interpreted as indicative of dome destruction. The vertical succession of alternating massive and stratified beds was instead interpreted as the occurrence of dilute PDCs due to hydromagmatic activity (Espíndola et al. 2000).

Apparently the crater remained open for the next 600–700 years, after which another explosive

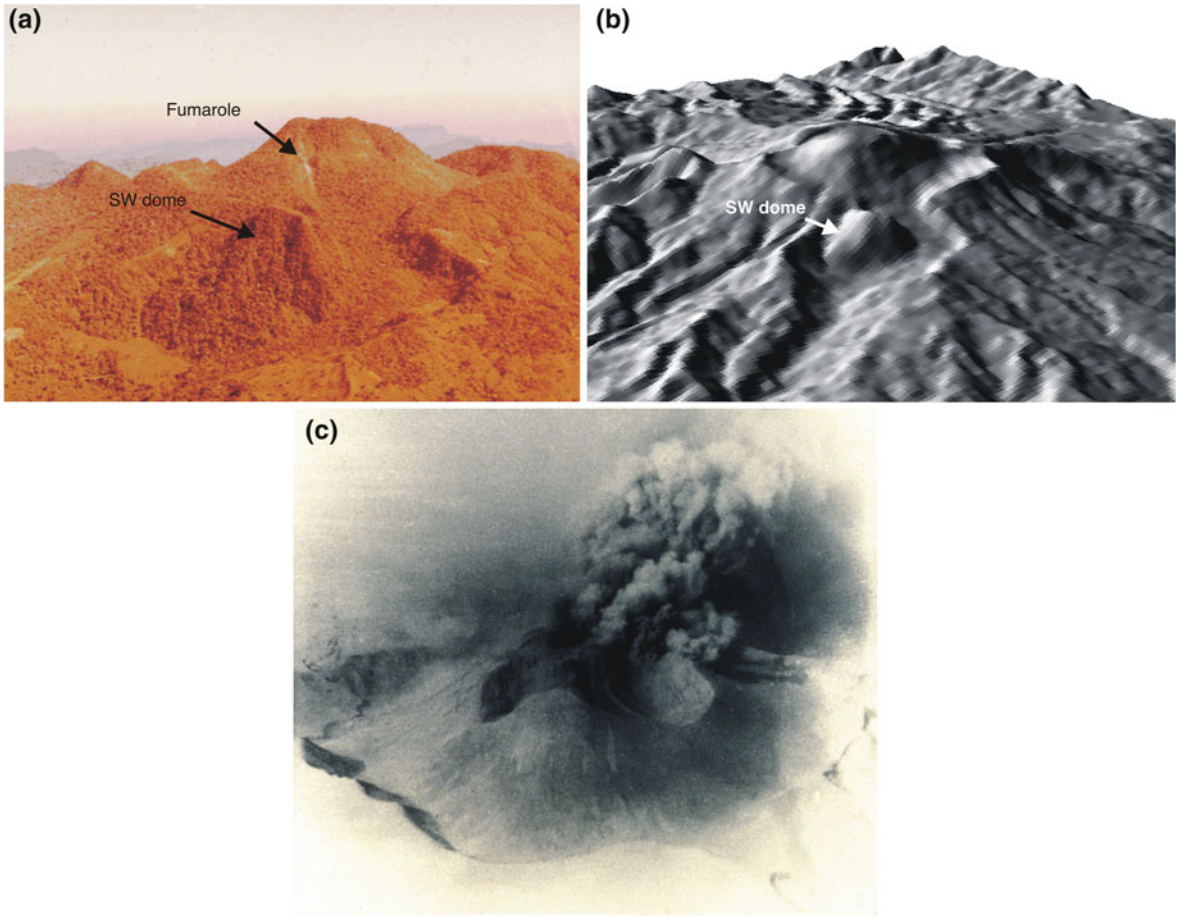

Fig. 3.5 **a** View toward the SW of the central dome inside the Somma crater, before the 1982 eruption. Note a white fumarole (*arrow*) along a vertical fracture on the central dome. The SW dome is visible in the foreground. Photo by René Canul in 1981. **b** Digital Elevation Model of the pre-eruptive topography, from the SW. **c** *Aerial view* toward the W of the central dome partially destroyed after the events occurred the night of 28 March (2315 local time). The photo was taken sometimes before April the 3rd, 1982. *Courtesy* of R. Tilling, *Geof. Int*. (2009)

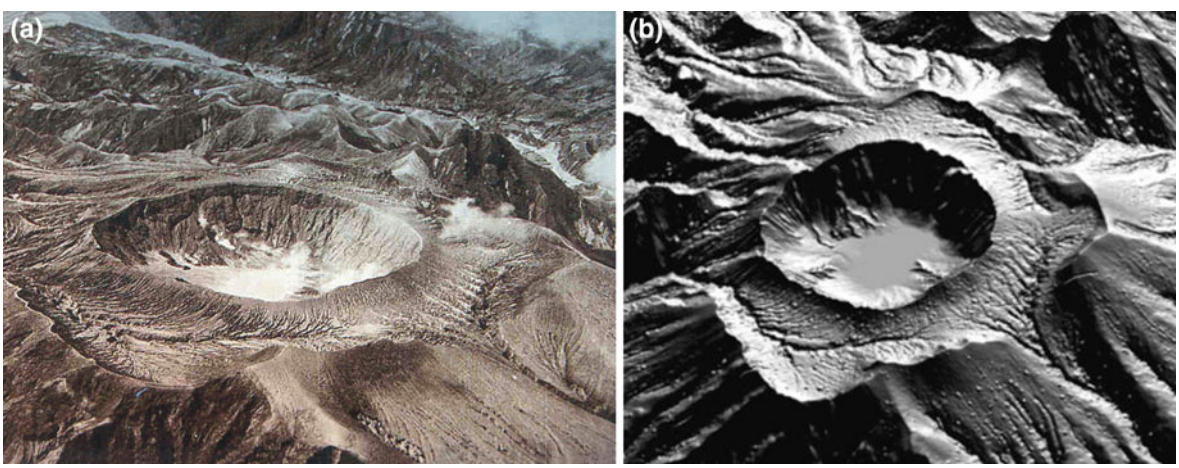

Fig. 3.6 **a** *Aerial view* from the S-SE of the volcano in May 1982, showing the newly formed crater ~1 km in diameter. *Photo* by GYMSA SA de CV. **b** DEM from the S-SE of the post-1982 eruptive topography

eruption, involving the collapse of low-altitude column that fed lateral density currents, occurred. Field evidence for this period of activity consist of a massive, dark-brown, matrix-supported deposit, with scarce lithic fragments and rounded altered coarse pumice lapilli, which contain abundant pottery fragments (**Unit I**, Espíndola et al. 2000) that crops out at distance of 3 km from the present crater, inside El Platanar valley. Charcoal sampled at different locations inside the deposit, yielded ^{14}C ages between 2470 ± 50 year BP (2464–2553 cal year BP) and 2645 ± 55 year BP (2732–2797 cal year BP). A paleosol overlying this deposit yielded ages between 2205 ± 60 (2218–2311 cal year BP) and 2290 ± 250 year BP (2041–2546 cal year BP), attesting the quiescence of the volcano after this eruptive phase.

Around 2,000 year BP, eruptive activity resumed, as indicated by deposits found at distances of 2.5 and at 4 km from the crater inside El Platanar valley (**Unit H**, Espíndola et al. 2000). At lower distances (2.5 km) from the crater, a massive deposit of coarse to medium ash (10–40 cm thick) at the base is separated through an erosive surface from an overlying pink massive deposit of coarse ash (30 cm thick), containing abundant andesitic lapilli, with vertical fumarolic pipes. Charcoal inside the deposit yielded ^{14}C ages of 2040 ± 125/120 year BP (1866–2153 cal year BP). The vertical succession ends with an alternation between massive beds of coarse ash and lapilli, cross-stratified beds of coarse ash and lapilli and massive beds of fine ash displaying load structures and containing ash aggregates. At greater distances (4 km), this unit consists of alternating stratified and massive beds of coarse ash and lapilli, capped by an upper bed of fine ash containing ash aggregates. Charcoal fragments found inside this succession, yielded ages of 2025 ± 85 year BP (1889–2066 cal year BP), and were attributed to the lateral transition of the ones described at shorter distances along the same ravine by Espíndola et al. (2000). Nevertheless, the deposit distribution and their structural and textural characters do not allow a single interpretation of the events. In fact, the fine ash gray massive bed at the base of the sequence could have been deposited either by currents generated during an initial hydromagmatic activity (as suggested by Espíndola et al. 2000), but may also represent the product of an early low-concentrated ash cloud that traveled ahead of a denser, more competent portion of a pyroclastic density current, which was preserved in some places, and eroded elsewhere by the following current. The presence of elutriation pipes inside this deposit indicates the occurrence of clasts segregation after deposition caused by gas escaping following the rapid settling of clasts. This stratigraphic succession could therefore record either the product of an initial hydromagmatic activity followed by a low pyroclastic fountaining which generated dense PDC (s), when the access of water was temporarily unavailable, or the spreading of a current generated by a pyroclastic fountaining from a low eruptive column produced by magmatic activity. Apparently, the explosive interaction between magma and water followed, producing more dilute PDCs, as recorded by the uppermost portion of the stratigraphic succession closer to the crater consisting of cross-bedded deposits of coarse and fine ash that shows load structures and ash aggregates (Espíndola et al. 2000). These last currents were poorly confined by the topography, and reached up to 4 km to the E. The succession of alternating stratified and massive beds, would record the instability of the flow downstream during its final spreading, which was followed by a final settling of ash, as attested by the capping ash aggregate-bearing layer. The water source responsible for this activity derived either from a crater lake (as suggested by Macías et al. 2008) or from a phreatic layer below the crater.

Around 1,800 year BP other episodes of explosive activity occurred, as indicated by radiocarbon dating on two paleosols, which bracket a light brown ash layer at distances of 1.5 km E from the crater that yielded ages between 1885 ± 75 year BP (1723–1896 cal year BP) and 1720 ± 70 year BP (1548–1707 cal year BP). This deposit was attributed by Espíndola et al. (2000) to the emplacement of a current rich in condensing steam (i.e. wet surge), and was correlated with a brown massive deposit, rich in andesitic lithic and pumice lapilli that crops out further downstream, 4.3 km to the E, with C^{14} ages of 1780 ± 95 year BP (1602–1820 cal year BP) (**Unit G** of Espíndola et al. 2000). The stratigraphic succession alone does not allow a unique interpretation of the events. In fact, the ash-rich layer bracketed by paleosols, could alternatively represent the fallout associated to the massive deposit found downstream, produced when the PDC generated by a magmatic activity was waning, which was preserved only at

some places. Another massive dark-gray deposit, 5 m thick, rich in dark gray andesitic and hydrothermalized lithic clasts (**Unit F**), exposed 2.5 km SW of the crater inside Agua Tibia gully, and dated at 1695 ± 65 year BP (1534–1636 cal year BP), would record another episode of explosive activity occurred 100 years later, under open vent conditions according to Espíndola et al. (2000). For this same lapse of time Tilling et al. (1984) reported two PDCs and associated fall layers, followed by debris flows (**Unit D**), between 1870 ± 70 (1721–1878 cal year BP) and 1580 ± 70 year BP (1395–1538 cal year BP). The occurrence of a paleosol between unit F and G (PFG of Espíndola et al. 2000) dated at 1720 ± 70 year BP would indicate that these deposits were generated during different eruptive events (i.e. around 1,800 and 1,600 year BP), separated by a significant lapse of time. The interpretation of these stratigraphic units (F and G) is not straightforward, and even if the occurrence of hydromagmatic activity was invoked (Espíndola et al. 2000; Macias et al. 2008), considering the descriptions provided by Tilling et al. (1984), the deposits would be better interpreted as the product of the collapse from low-altitude column(s). Nevertheless, for both stratigraphic successions, more detailed studies are needed to assess better the nature of events that occurred.

Another dome probably grew inside the crater and was explosively destroyed around 1,500 year BP. This activity was inferred considering the presence of a 4 m-thick gray, massive deposit of dark gray trachyandesitic and red hydrothermalized lithic blocks, in a matrix of coarse lapilli, with abundant fumarolic pipes (**Unit E** of Espíndola et al. 2000), which crops out 2 km E from the crater inside El Platanar valley. This deposit was correlated with a 5 m thick succession of cross-stratified, pumice-rich beds and massive beds, that crops out at 4.5 km E in the outskirts of the former Volcán Ch. village, dated between 1465 ± 95 (1291–1418 cal year BP) and 1490 ± 45 year BP (1327–1409 cal year BP). A similar age of 1520 ± 75 year BP (1343–1423 cal year BP), was obtained for a brown deposit of fine ash rich in pumice and carbonized tree branches found 2.5 km E, which overlies a green massive deposit of fine ash interpreted as the product of hydromagmatic activity. Based on the similar ^{14}C ages, these deposits were attributed to the same period of activity.

After 250 years, the activity resumed from an open conduit, as indicated by the stratigraphic record inside El Platanar valley and radiocarbon dating. Espíndola et al. (2000) described at distances of 2.5 km E from the crater a sequence of deposits consisting of a massive bed (20 cm thick) of brown fine ash at the base, overlain by a massive, 3 m-thick gray deposit of coarse ash rich in andesitic blocks, followed by 4 bedsets of light-gray massive coarse ash and pumice lapilli overlain by fine ash fall. Charcoal embedded in this deposit was dated at 1225 ± 105 year BP (1059–1270 cal year BP/680–891 AD) (**Unit D**, Espíndola et al. 2000; **Unit C** of Tilling et al. 1984). This vertical succession was correlated downstream, at 4 km, with a massive brown deposit of coarse ash. Tilling et al. (1984) described a Plinian pumice fall at the base of this sequence. Pottery shards found in the paleosol that overlies this deposit (Tilling et al. 1984), and small pieces of obsidian blades embedded within this unit (Espindola et al. 2000), were attributed to the Late Classic or Early Post classic period (A.D. 800–1200 probably as 1400 A.D). The fallout at the base described by Tilling et al. (1984), which was not observed in later studies (Espíndola et al. 2000), points toward the generation of a Plinian column that later collapsed to produce several PDCs, as attested by the occurrence of bedsets of massive coarse beds overlain by fine ash fallout. Apparently the crater remained open and, around 900 year BP, other pumice-rich current(s) were generated by column collapse(s) from sustained currents. Eventually pumice clasts fell inside the current without being registered as a fallout deposit. Field evidences for this kind of activity consist of massive, light-gray clast-supported deposits of lapilli and blocks of white pumice with minor coarse ash observed up to 3 km to the E, inside El Platanar valley, and up to 2 km to the N of the crater, in deep ravines, ranging in thickness between 1 and 15 m (**Unit C,** Espíndola et al. 2000). Charcoal sampled within this unit yielded ages between 845 ± 75 (686–798 cal year BP/1153–1264 AD) and 900 ± 90 year BP (739–835 cal year BP/1115–1211 AD). Ages of 795 ± 50 year BP (674–741 cal year BP) were obtained for the paleosol overlying this unit.

Explosive activity resumed around 550 ± 60 yBP (519–561 cal year BP/1389–1431 AD), as indicated by radiometric ages obtained from charcoal fragments inside a gray, massive deposit of fine ash, rich in pumice and crystals at the base of a widespread yellow pumice fall deposit (**Unit B**, Espíndola et al. 2000).

This fallout deposit covers an approximate area of 350 km^2 according to a 10 cm isopach, and overlies

Tertiary claystones to the SE and NW or, locally, a dark brown paleosol, containing abundant pottery shards, which developed on top of unit D (Espíndola et al. 2000).

Unit B is a clast-supported deposit consisting almost entirely (95 vol%) of yellow pumice blocks and lapilli (whitish on fresh surfaces), with rare gray and banded pumice lapilli, loose crystals, and gray claystones from the local basement. Dark gray mafic enclaves (44 wt% SiO_2) and amphiboles cumulates, occur either as fragments inside pumice clasts or as loose debris inside the deposits (Macías et al. 2003). All pumice samples are trachyandesitic in composition, with no compositional variation between yellow (55.1–55.4 wt% SiO_2) and gray (55.7 wt% SiO_2) pumice. The differences in color were attributed to larger proportions of hornblende in the gray pumices and a lower vesicularity (51–58 vol%) with respect to yellow pumices (63–74 vol%, Macías et al. 2003). The best outcrops are located between 5 and 10 km to the E and the S from the crater in the outskirts of Volcán Chichonal, Chapultenango and Carmen Tonapac villages (Fig. 3.7), while beyond 13 km most of the deposits have been removed by erosion. A maximum thickness of 110 cm was measured 3 km NE from the crater. Isopachs of this pumice fallout show two main dispersal axes. Close to the crater (<4 km) the dispersal is to the E, beyond 4 km, the dispersal shifts to N30°E (Macías et al. 2003). According to Macías et al. (2003), an area of at least 1,475 km^2 was covered by 1 cm of fallout during this eruptive event, which emitted an estimated volume of 2.8 km^3, corresponding to 1.1 km^3 DRE. Assuming an average density of 2.5 g/cm^3 for the lithic fragments inside the deposit, Macías et al. (2003) calculated a column height of 31 km. Based on this column height and assuming an eruption temperature of 800 °C, they estimated a mass eruption rate of 10^8 kg/s.

3.2.3 1982 Eruption

After the plinian event occurred around 550 yBP, a 1260 m a.s.l. a trachyandesitic dome was extruded within the Somma crater. A ring depression (moat) separated its basal talus breccia from the Somma crater (Fig. 3.5a, b). Apparently a lava flow flowed laterally from the dome on the western flanks of the Somma, reaching a distance of 1.5 km (Macías et al. 2010; Fig. 3.2a). This activity has been not yet well constrained in time, even though both the mineralogical association of the lava, and its stratigraphic position, suggest that a minor episode of effusive activity occurred sometime during/after dome emplacement.

Since the volcano had recorded no historical eruptions, no monitoring system existed in the area prior to 1982, except for a seismic telemetered network, installed in July 1979, at distances between 27 and 62 km from the vent, to monitor the impounding of a nearby dam (Chichoasén) by the CFE. Only the data from this local network were available to determine the onset of the eruption in later analyses (Haskov et al. 1983) before the installation of portable smoked-paper seismographs closer to the volcano by researchers of Universidad Nacional Autónoma de México (UNAM), who arrived in the area shortly after the beginning of the eruption (De la Cruz Reyna and Martín Del Pozzo 2009; Chap. 5).

A post-eruption review of available seismic records indicated that seismic precursors began in January 1980 and probably even in late 1979 (Jimenez et al. 1999). In September 1980, Canul and Rocha (1981) felt earthquakes during their fieldwork in the area. Nevertheless, their warning about a possible eruption reported to CFE remained unpublished, and therefore no preventive measurements were taken (Tilling 2009). In the months and weeks preceding the eruptions, local residents experienced several earthquakes (up to 30 events in 24 h on March 6, 1982), but the authorities did not act on their reports.

The reconstruction of eruptive events was obtained combining seismic data with available information from geostationary satellites. Eyewitness accounts provided additional observations to understand the succession of events inferred by the interpretation of the stratigraphic succession.

According to seismic records (Haskov et al. 1983), the eruption began on March 29 at 0515 UT (March 28, 2315 local time; UT = Local time-6 h) and lasted 32 min (Table 3.1). Local witnesses report this event later in time (i.e. at 0532 UT, Table 3.1). Geostationary satellites detected an eruptive column rising around 0600 UT, which according to infrared images, was 1 km above the 16.5 km-high tropopause 4 h later (Matson 1984; SEAN 1989). A dense plume drifted to the ENE, following the upper tropospheric circulation, while a less dense plume was dispersed to WSW following stratospheric winds (SEAN 1989;

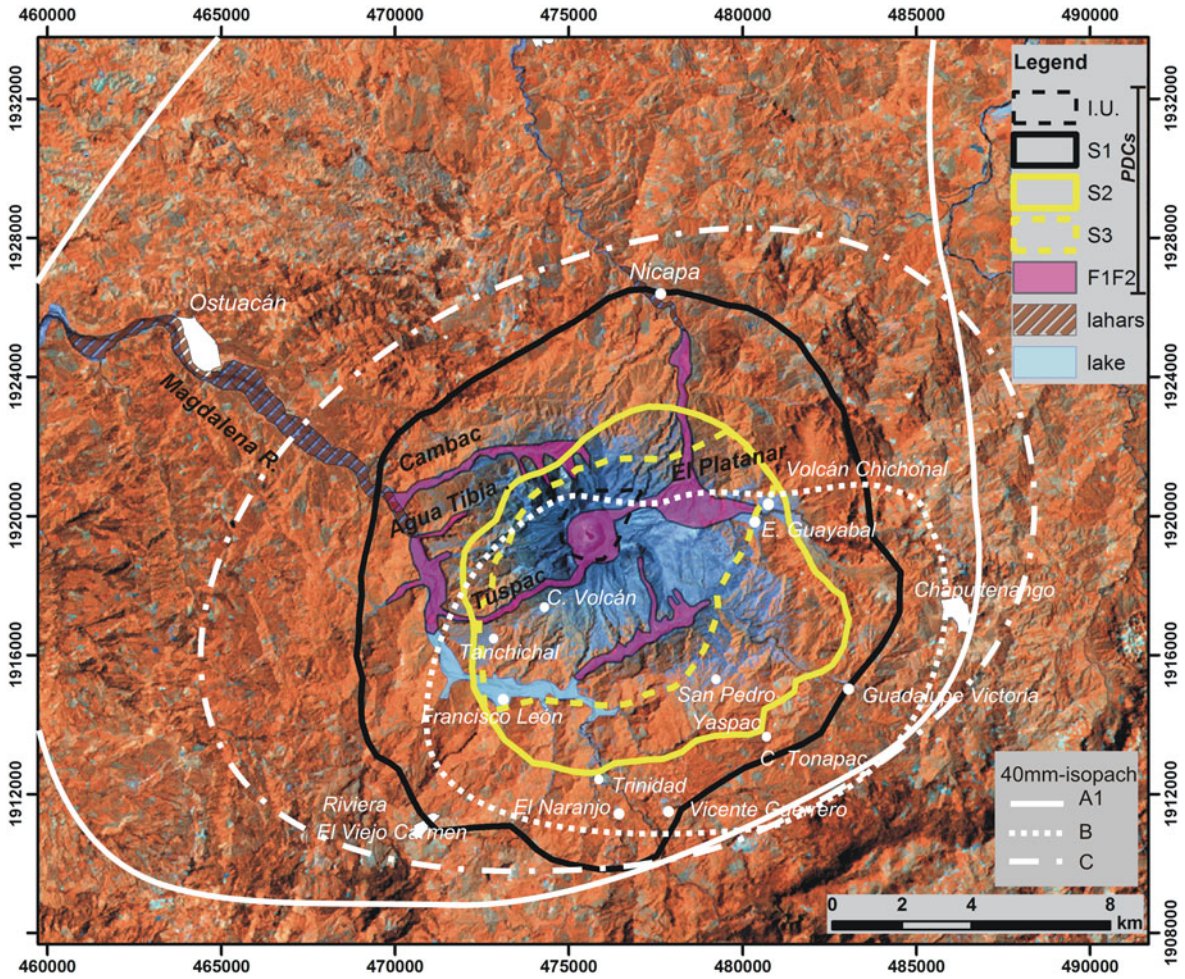

Fig. 3.7 A real distribution of the deposits generated during the 1982 eruption on a LANDSAT image. Isopachs of fallout deposits are drawn according to Carey and Sigurdsson (1986). The distribution of pyroclastic density current deposits (PDCs) is modified from Scolamacchia and Macias (2005). The extent of the temporary hot lake formed (by natural pyroclastic dams) at the confluence between the Tuspac and the Magdalena rivers is also shown. Dam failure on 26 May generated floods and lahars, the distribution of which is drawn according to Macias et al. (2003)

Table 3.1). A sulfur dioxide cloud was detected above the volcano by the Total Ozone Mass Spectrometer (TOMS) mounted on geostationary satellite (Krueger 1983; Krueger et al. 2008). A complex sequence of infrasonic signals with the occurrence of a strong gravity wave was recorded in Texas (Mauk 1983) by microbarographs and long period seismographs (Table 3.1). This event destroyed 1/4 of the dome (Fig. 3.5c), and deposited a normal-graded fallout deposit of trachyandesitic pumice lapilli, loose crystals of plagioclase, hornblende, and clinopyroxenes, with scarce lithic fragments (Fig. 3.7, fallout **A1** of Sigurdsson et al. 1984). The low content in lithic fragments, and the high degree of clast fragmentation were considered indicative of the occurrence of a phreatoplinian event (Sigurdsson et al. 1984). The polymodal grain-size distribution of this layer was attributed to the occurrence of aggregation processes during fallout (Varekamp et al. 1984). The maximum column height was estimated to be 27.3 km (Carey and Sigurdsson 1986).

Several eruptive events occurred between March 30th, and April 2, some of which reached the middle and upper troposphere according to satellite records (Matson 1984; SEAN 1989), and were seismically detected (Haskov et al. 1983), but they did not produce

significant deposits according to eyewitness accounts (SEAN 1989).

The eruptive activity resumed early in the morning of April 3 between 0837 and 0840 UT as indicated by seismic records (Haskov et al. 1983). Eyewitness accounts from Chapultenango village, 10 km SE from the crater, reported lightening inside a vertical column at 0830 UT (Albarrán 1983), followed after 15 min by pumice fallout (Table 3.1).

In Texas, atmospheric pressure disturbances were registered by microbarographs in the form of complex infrasonic signals, at 0850 UT (Mauk 1983). A strong gravity wave indicated that the eruption column penetrated the tropopause (SEAN 1989). At 0900 UT (0300 local time) a rising plume was observed by geostationary satellites, and dispersed toward the E–NE (Matson 1984). According to estimates by Krueger et al. (2008) as much as 310 ktons of SO_2 were released into the upper troposphere during this eruptive event. A haze of SO_2 was visible during the day on the NE flank of the volcano (SEAN 1989). These reports attest to the occurrence of a plinian event which, according to Sigurdsson et al. (1984) deposited a minor fallout of fine ash (**A2**; Fig. 3.7 and Table 3.1), with a limited distribution and small volume. This layer was not recognized as a distinctive separate fallout deposit in the stratigraphic record in other studies (Varekamp et al. 1984; Scolamacchia and Macías 2005).

Eventually, other eruptive events occurred early in the morning of April 3, as evidenced by a complex succession of infrasonic signals registered for 27 min at Mc Kinney, Texas, starting at 0912 UT (Mauk 1983; SEAN 1989). They were also seismically detected between 0925 UT and 1040 UT (Haskov et al. 1983). The energy release for these explosive events was estimated at the equivalent of 99.5 ktons TNT and was characterized by a pulse of high frequency, high mode number infrasonic signals "similar to those produced by atmospheric nuclear weapons tests" (Mauk 1983). According to stratigraphic records, this succession of eruptive events began with high energetic explosion(s) triggered by the interaction between the rising magma with an active hydrothermal system and groundwater (Scolamacchia and Macías 2005). This event likely caused the destruction of a great portion of the remnant dome. It generated a PDC rich in hydrothermally altered lithic fragments, liquid water, and hydrothermal fluids, strongly erosive on the underlying fallout deposits and the soil beneath, which reached distances up to 6.3 km to the S, and 5 km to the N. Field evidences for this event are represented by a poorly sorted massive deposit of accidental hydrothermalized lithic blocks immersed in a matrix of coarse ash and lapilli consisting of yellowish rounded pumice, poorly vesiculated glass, loose crystals of plagioclase, hornblende, augite and minor oxides (S1–0 of Scolamacchia and Macías 2005). Pieces of overturned soil were observed embedded in this deposit (Sigurdsson et al. 1984). The presence of soil stripped from the underlying surface has been described also at the base of deposits produced by high-velocity currents (i.e. layer A0 of Fisher 1990) following the sudden decompression of a dome or cryptodome ("directed blast", e.g. Gorshkov 1959, 1963; Hoblitt et al. 1981; Moore and Sisson 1981; Fisher 1990; Belousov et al. 2007). Even if the distribution of S1–0 elongated in a N-S direction, most likely reflecting topographic control, and the possibility of a lateral explosion are unlikely, the textural and structural characteristics observed suggest that the initial event was highly energetic.

S1-0 can be correlated with the "brown massive surge layer" described by Sigurdsson et al. (1984) in the Nicapa valley, ~4 km NE of the crater. This deposit also contains aggregates of different shapes (i.e. irregular clusters, and spherical pellets with a solid core of pumice or crystals, following the nomenclature of Brown et al. 2012), consisting of poorly sorted mixtures of mm-sized pumice, and 100 μm-glass and crystals, cemented by a Fe-S-rich, orange-red film that represent up to 60 wt% of size fractions between 1 and 5 mm. Shortly afterwards, closely-spaced hydromagmatic events due to the interaction of variable proportions of magma and groundwater generated diluted PDCs (i.e. pyroclastic surges) that spread almost radially from the crater (S1–1 to S1–7 of Scolamacchia and Macías, 2005), reaching distances of 9.5 to the NE, 10.5 km to the E, 4.5 km W, and 8.5 km S. They were highly destructive up to 7 km E–SE, and 8 km S (Sigurdsson et al. 1987; Scolamacchia and Macias 2005). The deposits produced by these events are in general buried by deposits of later eruptive activity, except at distances greater than 5 km, and can be observed only in trenches dug under the present surface (Fig. 3.8a). The structural and textural characteristics of the deposits that open the sequence (S1–1, S1–2 of Scolamacchia and

Table 3.1 Chronology of the major events of the 1982 eruption, according to seismic and satellites records, eyewitness accounts, microbarographic acoustic signals recorded from far away stations, and stratigraphic analyses

Date	Seismic records	Eyewitness accounts	Satellite records	Other records (registered worldwide)	Inferred deposits
March 29	0515[a]	**0532** (1132 March the 28th, local time)	Eruptive plume 1 km above the 16.5 km-high tropopause, 4 h after the beginning of the event[g]. **1816** SO_2 cloud observed on the NW side of the volcano, spreading E and W, by TOMS[h]. Total mass of SO_2 in the clouds estimated at 0.72 Tg[h]	**0532** complex sequence of infrasonic signals registered in Texas (event 088[e]) and Antarctica[d]. Energy released 0.26 MT[e]. Occurrence of a strong gravity wave indicated that the er. plume penetrated the tropopause	Fallout A1
April 3	0840[a]	**0830** from Chapultenango (10 km SE) lightening observed inside a vertically rising eruptive cloud, followed 15 min after by fallout of pumice lapilli (up to 3 cm)[c]. Fallout continued for 45 min with a decrease in particle dimension[c]	Eruptive column emerging from the volcano at **0900**, and blew to the NE and SW[d, g]	**0850** Pressure disturbances in Texas (event 093A[e])	Fallout A2 (minor)[f]
			Total mass of SO_2 estimated to be 310 k tons[h]	Gravity waves indicated that the eruption plume penetrated the tropopause	
				Energy released 1.06 MT[e]	
April 3	0925–1040 1003 major event[a]	The inspection at Volcán Ch. village (4.7 km E) ≈8 h after from the previous event (around 1650, April 3) indicate downed trees and houses in E–SE direction; presence of a 80 cm thick deposit; T at the surface 60 °C, increasing toward the center[c]; 7.5 cm of new ash reported at Nicapa (7.5 km NE)[d]. At **0030** April 4 only small gas plume observed	No data available at 1200[g]	**0912** (event 093B[e]) complex acoustic infrasonic signals similar to nuclear tests. Total duration 27 min[e]. Energy released estimated at 99.5 kT[*e]. No evidence of gravity waves	S1, PF1, IU
April 4	0139 major event[a]	**0130**[c] from **Chapultenango** (10 km SE) "mushroom shaped cloud", with lightening vertically rising. Fallout of pumice blocks (40 cm) and lithics (10 cm) began after 10 min. Two "nuée ardentes" observed, one moving toward the W[c]	**0400** NOAA geostationary satellites detected eruptive plume at heights <16.9 km[g]. Plume spread NE, following tropospheric winds and SW following stratospheric winds[d, g]. Ash drifted toward Guatemala and Belize for the next 5 h[d]	**0200** (event 094[e]) infrasonic signals registered in Texas, exciting initial gravity waves, and a complex series of acoustic wave for ~48 min, attributed to the occurrence of distinct explosions every 2–3 min[d]	Fallout B, PF2, S2
		0135 from **Ostuacán** (11.5 km NW) heavy electrical activity inside a vertical cloud. Seismographs saturated for 20 min. Moderate fallout from >1 h.[a, b] Advancing flow toward W[b]		Energy released estimated at 1.14 MT[*e]	
		A pumice flow deposit, observed 5 km from the summit to the NE, terminating 2 km from			

(continued)

Table 3.1 (continued)

Date	Seismic records	Eyewitness accounts	Satellite records	Other records (registered worldwide)	Inferred deposits
		Nicapa. At the distal end was about 3 m thick. Pumice blocks up to 1 m. On April 8, T measured by thermocouples at 40 cm depth averaged 360 °C, high as 402 °C			
		The pumice flow appeared to have been emplaced by 2 events in rapid succession[d]			
April 4	1110 (start)	**1122** plume reported from ground observers[d.]	**1130** first appearance of the plume on geostationary satellites[d]	**1122** (094B event[e]) Infrasonic signal registered in Texas and Antarctica. Duration of the signal > 150 min	Fallout C, S3
	1215 (end)[a, b]	**1132** from Ostuacán onset of the eruption due to continuous rumbling. Felt earthquakes. Pumice fallout started at **1143** and continued until **1200**[a]	**1144** eruptive plume recorded by NOAA polar orbiting satellites[g]	Complex signal (similar to 093B) composed of several modes of infrasonic excitation, indicative of two major explosions separated early in the sequence by 8 min, followed by a series of distinct events separated in time by 3–5 min[i]. Energy release two orders of magnitude >093B. Bichromatic LP Rayleight waves and coupled air waves, registered worldwide by gravimeters and very long period seismic stations, after 1100 UT[e]. Main energy release occurs in less than 1 h[e]	
	Tremor-like activity recorded in Mexico City (≈700 km N)	In Pichucalco (20 km NE) incandescent tephra rising from the volcano. The ash cloud darkened the sky during the morning	Infrared image 3.5 h later, show the top of the plume at 16.8 km		
		Ash flow downed the trees in the Nicapa valley, and left a relatively thin layer of ash, with a T of 94 °C at 10 cm depth, measured 3 days later[d]	Total Ozone Mass Spectrometer (TOMS), detected a great sulfur dioxide cloud on the volcano and trailing off to the E. Estimated mass of SO_2 at least 3.5 Tg[h]		
		Extreme heat radiating from the deposits made impossible to reach the village of F. Leon (5 km SW from the crater). Between Ostuacán and F. Leon a river boiling and downed trees could be seen upslope[d]			
April 5		Activity lasting 3 h. No incandescent tephra ejected[d]	**1730** plume rising observed by satellites		S4, S5[j]

All times are UT (Universal time = local time + 6 h) * 1kT $\sim 4.22 \times 10^{19}$ ergs

[a] Haskov et al. (1983)
[b] De la Cruz and Martin Del Pozzo 2009
[c] Albarrán (1983)
[d] SEAN (1989)
[e] Mauk (1983)
[f] Sigurdsson et al. (1984)
[g] Matson (1984)
[h] Krueger et al. (2008)
[i] Widmer and Zürn (1992)
[j] Macías (1994)

Macías 2005), such as irregular contacts between beds produced by the load of damp deposits on other ones still plastic beneath, laterally discontinuous lamination, the presence of vesicles, the plastering against steep walls indicate that the events occurred at the beginning involved significant quantities of water in contact with magma, producing currents rich in condensing steam (i.e. wet surges), as observed elsewhere (e.g. Lorenz 1974; Sohn and Cough 1992; Cole et al. 2001; Sohn et al. 2012; See Inset Box). Also in S1–1 and S1–2, 10–40 wt% of components in grain-sizes between 8 and 1 mm consist of aggregates of different shapes (irregular clusters, spherical and elongated pellets with or without a core of crystals, pumice, or organic fragments). Individual components of the aggregates are crystals and glass fragments hundreds of microns in size, and mm-sized pumice, cemented by a red-orange film with an overall poor sorting. Gradational variations in grain size, determine a weak internal layering (Scolamacchia et al. 2005). The composition of the cementing film consisting of abundant S and Fe with minor P was attributed to the interplay between magmatic and hydrothermal fluids in different amounts (Scolamacchia et al. 2005).

The availability of water entering in contact with magma apparently was reduced thereafter, (e.g. Sheridan and Wohletz 1981, 1983a, b; Kokelaar 1986; Zimanowski et al. 1997a; Zimanowski 1998; Büttner et al. 1999; Zimanowski and Wohletz 2000) as attested by the textural and structural characters of the deposits, generating a PDC (i.e. dry surge) that was mainly dispersed up to 5 km to the eastern and northern sectors of the volcano and up to 7.5 km to the S. This PDC was able to carbonize wood, attaining temperatures of 360–400 °C (Sulpizio et al. 2008), and to partially or completely erode deposits from previous activity, including topsoil and sedimentary rocks of the Tertiary basement (Sigurdsson et al. 1984). It deposited a coarse-grained reddish bed of coarse pumice lapilli and minor hydrothermalized lithics from the central dome, immersed in abundant ash (S1–3, Fig. 3.8b–c). Small-magnitude events due to an increase in the amount of water entering in contact with magma followed, producing dilute PDCs that deposited a succession of multiple laminae, slightly different in color, grain-size and degree of vesiculation with a patchy distribution up to 3 km to the E-SE (S1–4–5–6). Aggregates (spherical pellets and irregular clusters) either cemented or not by a red-orange film, occur as components (10–40 wt%) in S1–5 and S1–6 in size fractions between 1 and 8 mm, beside white pumice, poorly vesiculated glass, and crystals (Scolamacchia et al. 2005). The following eruptive event involved less amount of water producing a dilute PDC (dry surge) with a high erosive power at distances between 3.5 and 4.7 km from the crater to the E-SE that reached the village of El Naranjo 8 km S (Fig. 3.7). Field evidences for this event consist of a light gray deposit of pumice lapilli and blocks in a matrix of coarse ash, with minor accidental lithics from the former dome (S1–7, Fig. 3.8d), with a maximum thickness of 90 cm in topographic lows at 3.5 km SE from the vent. At Esquípula Guayabal, 3.5 km SE from the crater, this current was able to pick up and displace at least locally, concrete blocks 47 × 15 cm (Scolamacchia and Shouwenaars 2009). Other objects (e.g. steel reinforced bars of houses foundations), embedded in this deposit, were observed bent in an E-SE direction. This current was able to erode completely 6 cm of fallout A1, at El Naranjo, 8.5 km S. The preservation of a fine ash layer on top of this deposit due to the fallout from the waning portions of the current (Fig. 3.8d) would indicate its cessation (e.g. Walker 1984; Branney and Kokelaar 2002) and a pause in the eruptive activity.

According to Sigurdsson et al. (1984) and subsequent studies to date, the succession of eruptive events described above started on April 4 around 0135 UT.

However, combining available eyewitness accounts with seismic, infrasonic records, and stratigraphic data, several evidences support the hypothesis that these powerful hydromagmatic events actually occurred a day earlier, during the early morning hours of 3 April (Scolamacchia 2012; Table 3.1):

(A) People returning to Volcán Chichonal (4.8 km E), from Chapultenango (10 km SE), several hours after the plinian event that occurred at ~0830 UT on 3 April, observed that trees had been downed in a ESE direction along the small road that connect the two villages; artifacts and houses in Volcán Ch. had been downed in the same direction (Table 3.1). The directional downing of trees and houses reported by eyewitness accounts, implies the passage of an energetic lateral load, which can be likely associated to the movement of the diluted PDCs described above.

(B) According to eyewitness reports, the village of Volcán Chichonal was already buried by a 80 cm-thick deposit made of "several light and dark

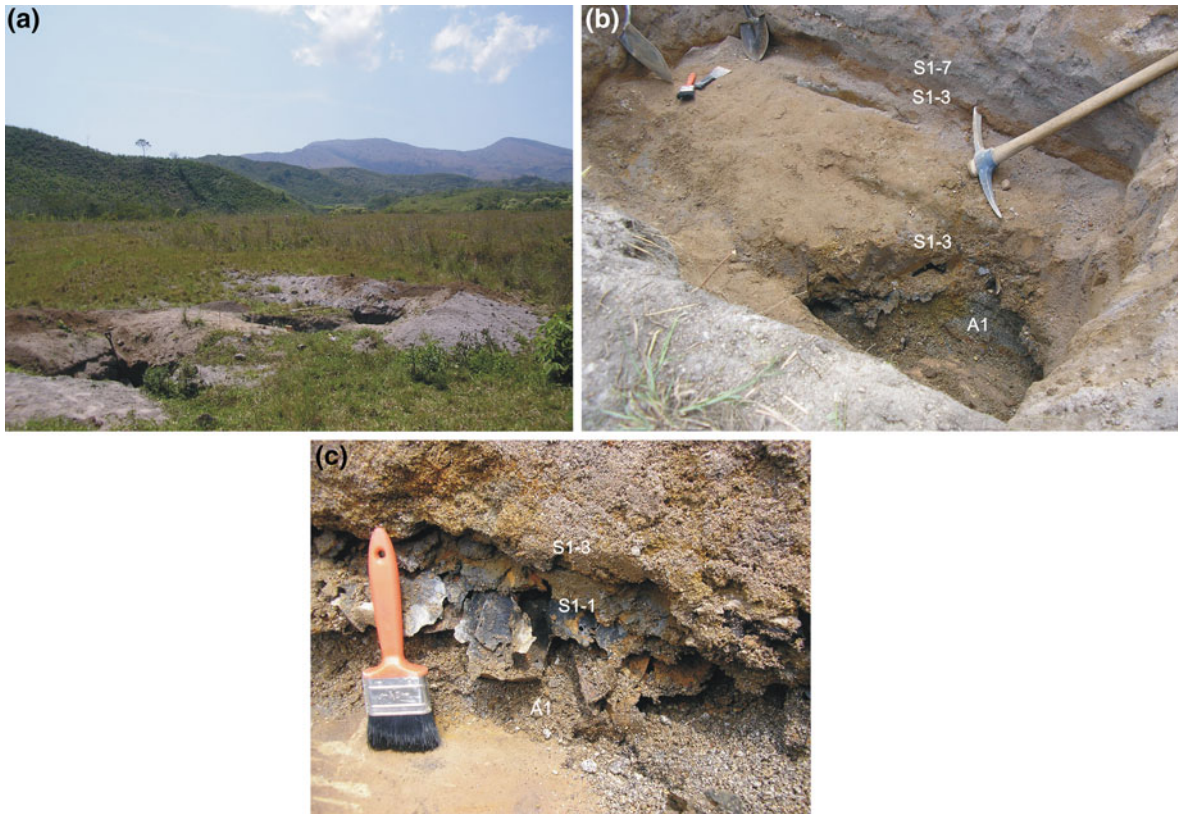

Fig. 3.8 **a** View of the former village of Volcán Chichonal, located 4.8 km E from the crater. Two trenches dug below the present ground surface are seen in the foreground. In the background are visible the eastern walls of the Somma crater. **b** Partial view of the deposits in one of the trenches (*Left* in **a**) showing the stratigraphic succession from *A1* to the lower subunits of *S1* (partial). **c** Detail of the lower portion of the trench in **b** showing fallout *A1*, overlain by the laminated roof of the collapsed church and by subunits *S1–1* and *S1–3*. **d** View of the complete succession of deposits in one of the trenches dug at Volcán Chichonal village (*left* in **a**). From the *base* to the *top* are visible subunits *S1–3* (*red*), *S1–7* (*gray*), fallout B, unit S2, fallout C, and several varicolored horizons of *S3*. Shovel for scale measures 67 cm. **e** Detail of the uppermost succession visible in the trench on the *right side* in **a**, showing the varicolored laminated deposits produced by the initial hydromagmatic events that alter the emplacement of fallout **c**, characterized by a high proportion between magma and water. Note the subtle discontinuous lamination of some of the layers and the subsequent erosion (2 cm) by a subsequent (*S3–7*) current ("dry" pyroclastic surge). **f** View of the succession of unit S3 deposited at Esquípula Guayabal, 3.5 km SE of the crater. The varicolored deposits at the *bottom*, reflecting the deposition from "wet" pyroclastic density currents, are partially eroded by the "dry" current *S3–7*. This situation is similar to what observed at Volcán Chichonal (in **e**). Note the succession of stacked inverse-graded pumice layers suggesting unstable, waxing conditions of the current at this location

horizons" some of which showed vesicular texture (Table 3.1); the temperature measured at the deposit surface was 60 °C (Albarrán 1983). These accounts suggest that other deposits, beside fallouts layers A1/2, had already been emplaced during early morning of 3 April. The descriptions of the textural and structural characteristics point toward the occurrence of diluted PDCs produced by magma-water interaction, as also suggested by the temperature measured at the deposit surface only few hours after their emplacement, which would indicate that the parent currents had temperatures <100 °C. The total thickness of fallout A1 and unit S1 measured recently in a trench dug at the former Volcán Chichonal village, is 49 cm (Fig. 3.8a–d). The difference in thickness with what was measured in 1982 can be likely attributed to the post-depositional compaction following the subsequent burial by later deposits.

(C) At 0912 UT on 3 April, microbarographs in Texas registered infrasonic signals that resemble those

Fig. 3.8 continued

produced by nuclear explosions (Mauk 1983; Table 3.1). Similar infrasonic signals were recorded also during most of the hydromagmatic events that occurred during the 1991 eruption of Pinatubo (Hoblitt et al. 1996; Tahira et al. 1996). The similarities existing between base surges generated during nuclear explosions (Young 1965) and those generated during hydromagmatic explosions, have been discussed in several studies (e.g. Richards 1959; Moore et al. 1966; Moore 1967), suggesting that the signals registered in Texas can be related to the hydromagmatic events described above.

Eventually, the removal of a great portion of the dome by the initial flashing of the hydrothermal system and the following phreatomagmatic activity promoted magma vesiculation by releasing the overlying pressure, and caused the generation of a low-altitude column, which collapsed with the formation of dense, lithic-rich, PDC(s) (PF1 of Macias et al. 1997; "lithic debris flow" of Sigurdsson et al. 1984). Such current(s) were partially confined by the Somma walls, where they left a 10 m-thick massive deposit rich in hydrothermal lithics at the base (Macías et al. 1997), but they were able to spread along major drainages to the N (Cambac), the SW (Tuspac), and the E-SE (El Platanar). At distances of 1–1.5 km E, a decrease in the Somma slopes from 11° to 3° resulted in a reduction in flow speed and the deposition of the

coarser load of the current, as attested by a massive breccia deposit rich in juvenile and lithic blocks up to 1.2 m in diameter (Macias et al. 1998). The flows were blocked at ~4 km distance by the Susnubac river (Fig. 3.7) perpendicular to flow direction (Sigurdsson et al. 1984). This event probably occurred around 1030 UT on April 3 (0430 local time), as suggested by a major peak observed in the seismic signals (Haskov et al. 1983). According to the stratigraphic record in proximal areas (Macías et al. 1997; Scolamacchia and Macías 2005), other minor eruptive events occurred shortly after the emplacement of PF1, due to the contact between groundwater and magma, producing PDCs that waned at distances of few hundred meters remaining confined inside the Somma crater (Lower IU). These events were followed by a more concentrated PDC, which emplaced a small-volume lithic-rich deposit (UI-3), which was followed again by a close succession of other hydromagmatic events (Upper IU) whose products, mainly contained by the Somma walls, reached maximum distances of 1.5 km to the NE. The types of aggregates found in the PDC deposits of Upper IU, and the degree of alteration of juvenile fragments, has been interpreted as the evidence that hydrothermal fluids were involved also during this phase of the eruption (Scolamacchia et al. 2005). However, no eyewitness accounts exist about these events, as they occurred early in the morning and were restricted to proximal areas, which were neither accessible nor explored.

Another eruptive phase began at about 0130 UT on April 4, according to eyewitness accounts from Chapultenango that described a vertical rising plume (Albarrán 1983), which also was observed from Ostuacán at 0135 UT (De la Cruz-Reyna and Martín del Pozzo 2009, Fig. 3.9) and registered by seismographs at 0139 UT (Haskov et al. 1983). Heavy fallout of pumice and lithic lapilli followed, lasting 1 h according to both reports (Haskov et al. 1983; Albarrán 1983; Table 3.1). Shortly after, currents moving on the ground toward the west were observed from Ostuacán (De La Cruz Reyna and Martín del Pozzo 2009) and from Chapultenango "moving laterally at high-velocity…without rising material" (Albarrán 1983). At 0200 UT, few initial gravity waves, and a complex succession of acoustic signals were registered in Texas for ~48 min and attributed to the occurrence of distinct explosions every 2–3 min (SEAN 1989; Table 3.1). At 0400 UT, geostationary satellites

Fig. 3.9 View of the crater of El Chichón from Ostuacán village (10.5 km NW) the evening of April 3, 15–30 min after 1935 local time (0135 UT). A *vertical* plume is glimpsed rising vertically from the crater, attesting the occurrence of what will be later identified as the Plinian event B. *Photograph* by Servando de La Cruz Reyna. Courtesy of the author

reported a plume elongated in a NE-SW direction (Matson 1984; SEAN 1989). Eventually, this eruptive phase began with the generation of a plinian column that penetrated the tropopause and emplaced a widespread gray to reddish deposit of slightly normal-graded white pumice, rich in hydrothermally-altered lithic lapilli (fallout **B**, Varekamp et al. 1984; Sigurdsson et al. 1984). Grain-size data and isopach maps, indicated that fallout layer B has the coarser proximal components among all fallout deposits of the eruption, and a moderate distal fine ash component. Based on the maximum lithic distribution, Carey and Sigurdsson (1986) concluded that this plinian event had the largest mass eruption rate (6×10^7 kg/s) among the fallouts produced in 1982, and calculated a maximum column height of 31.6 km. However, their calculated altitude is not confirmed by satellite observations (SEAN 1989), and the volume mapped on the ground would indicate a much smaller column height (21 km, according to Matson 1984). More recent estimates (Bonasia et al. 2012) using the Buoyant Plume Theory (Bursik 2001) implemented in the FALL3D numerical code (Costa et al. 2006; Folch et al. 2009) obtained a column height of 28 km for this plinian event.

The collapse of this eruptive column generated dense PDCs that were channeled through major valleys to the W, NE and N, following the volcano's drainages, as indicated by eyewitness accounts from Ostuacán and Chapultenango (Table 3.1). The deposits of this activity consist of 2–3 flow units of

massive, dark-gray, deposits of pumice lapilli and ash, more rich in lithic blocks inside the moat (Macías et al. 1997), where they partially ponded. The Magdalena river to the W, and the Susnubac river to the S, were able to block these flows (Sigurdsson et al. 1984), but no obstacles existed toward the NE, and the flows advanced up to 5 km along the El Platanar river (SEAN 1989; Table 3.1). Contemporaneous phreatomagmatic activity accompanied the collapse of the column, as indicated by the successions of one to four bedsets made up of a fining upward sequence of beds rich in white pumice lapilli and blocks with different structures, which become progressively finer-grained from the base toward the top that are intercalated to (S2-0), or directly overlie (S2-1, S2-2), pyroclastic flow PF2 (Scolamacchia and Macias 2005). They crop out discontinuously from the crater at distances greater than 1.3 km, covering an approximate area of 57.1 km^2 (Fig. 3.7). According to deposit distribution, these currents spread mostly to the eastern sector, following El Platanar river, and one affluent of the Susnubac river, and to the SW, along the Tuspac river, being strongly erosive on underlying deposits at distances between 3.5 and 5 km (Scolamacchia and Macías 2005; Scolamacchia and Schouwenaars 2009). To the E, they consist of a maximum of four bedsets, each one capped by a fine massive ash layer, attesting the emplacement of 4 different currents some of which were able to displace locally small tree trunks up to distances of 5.2 km E (Scolamacchia and Macías 2005). Components of finer fractions are white pumice and dense dark-gray trachyandesitic glass, loose crystals of plagioclase, augite, hornblende and minor sphene in different proportions as occur in other PDC deposits of the same eruption, beside a low percentage (2–3 wt%) of accidental altered clasts from the old dome. Weakly vesiculated glass with planar surfaces intersecting at high angles, (*blocky shapes*, Sheridan and Wholetz 1983a; Heiken and Wholetz 1985) is common in fractions finer than 125 μm (Scolamacchia and Macías 2005) indicating the occurrence of a brittle fragmentation of the melt at the contact with the water.

A final eruptive sequence started on April 4 at 1110 UT, according to seismic records (Haskov et al. 1983). Eyewitness accounts reported the start of this event between 1122 UT (SEAN 1989) and 1132 UT (Haskov et al. 1983). A rising plume was first recorded around 1130 UT by a NOAA geostationary satellite (Table 3.1). Heavy fallout of pumice lapilli started at 1143 UT, and continued for about an hour (Haskov et al. 1983). Infrared images indicated that an eruptive column penetrated the tropopause 3.5 h later (SEAN 1989). As a result of this activity, a widespread fall deposit of normal-graded white trachyandesitic pumice lapilli and crystals, with minor lithic content, was deposited in an ENE direction across 3,000 km^2 (fallout **C** of Sigurdsson et al. 1984). Based on a model of different transport direction in the tropospheric and stratospheric circulation, Carey and Sigurdsson (1986) calculated a column height of 28.8 km, attributing this event to a phreatoplinian activity. The vertical rising of this Plinian eruptive plume was registered worldwide by gravimeters and very long period seismic stations as bichromatic long-period Rayleigh waves and coupled air- waves (Widmer and Zürn 1992; Zürn and Widmer 1996). Based on infrasonic records, Mauk (1983) calculated that this event liberated an energy equivalent of 2.6 MT TNT in a complex sequence; gravity waves, induced by the thermal perturbations associated to the vertical rising of the plume, (Zürn and Widmer 1996), were followed by several high-frequency infrasonic pulses between 1309 UT and 1435 UT, which were attributed to the occurrence of distinct explosive events separated in time by a 3–5 min. Stratigraphic evidences indicated that after the deposition of fallout C, hydromagmatic activity was dominant, producing a series of diluted PDCs (unit S3 of Sigurdsson et al. 1984). Downed trees due to a "flow that left a thin layer of ash" were reported at distances of about 5 km to the NE after this event (SEAN 1989; Table 3.1). According to Sigurdsson et al. (1984, 1987) the deposits resulting from this activity were rapidly eroded due to heavy rains. Nevertheless, subsequent studies recognized deposits from these currents dispersed across an area of 44 km^2 (Scolamacchia and Macías 2005). This activity involved different proportions of water and magma. The resulting deposits consist respectively of varicolored, vesiculated layers of fine-ash and lapilli with discontinuous lamination, and of coarser-grained deposit of coarse ash, lapili and blocks which were strongly erosive on the deposits beneath and reached distances up to 4.8 km from the vent (Fig. 3.8e). Some of these currents were short-lived and vanished at distances of 2.5 km (e.g. S3-1-2 of Scolamacchia and Macías 2005) or were eroded by following flows. Others were of higher magnitude and traveled distances as far as 5 km E (e.g. S3-7). Irregular clusters,

consisting of pumice up to 6 mm in size and crystals, and minor spherical pellets (with or without a solid core) of glass and crystals cemented by a S-Fe-rich film, represent up to 90 wt% of the components of size fractions coarser than 4 mm in S3-3. They are abundant in deposits that crop to the E-NE between 2 and 3.6 km, and reduce consistently at distances greater than 4 km. To the S, aggregates are free of a cementing film, and characteristically smaller in dimensions (≤2 mm), with individual components ranging between 10 and 300 microns maximum (Scolamacchia et al. 2005). The hydromagmatic activity continued, producing alternating "dry" (T > 100 °C) PDCs, which were erosive up to 5 km to the ESE (e.g. S3-7-11-13 of Scolamacchia and Macías 2005) or "wet" (T < 100 °C) PDCs whose deposits, otherwise eroded, were preserved mostly in topographic lows at distances <2 km to the E (e.g. S3-8-9-10 and S3-12). These discrete, numerous, closely-spaced explosions generated surge-type pyroclastic density currents (e.g. Moore et al. 1966; Moore 1967; Kokelaar 1986; White 1991) that can be likely correlated with the infrasonic signals registered in Texas on April 4 after 1309 UT (Mauk 1983; Table 3.1), even if the time of eruptive events is only approximate considering the time lag existing between the eruptive events and the registered infrasonic signals. Similar infrasonic signals were registered during most of the hydromagmatic events preceding the climactic caldera collapse during the 1991 eruption of Pinatubo volcano (Tahira et al. 1996). Such signals were generally accompanied by an abrupt onset of high-amplitude tremor but, in some cases, no seismic signals were recorded (Hoblitt et al. 1996).

Minor phreatomagmatic events probably occurred during the following days, but their distribution remained confined inside the newly formed crater (Units S4 and S5 of Macías 1994, Table 3.1), and they were reworked/eroded during the following raining season.

The massive emplacement of pyroclastic deposits at the confluence between the Magdalena and the Tuspac rivers caused a rise of 30 m of the base of the thalweg of the Magdalena river (Macías et al. 2004). A 55-m thick dam formed 3.5 km downstream of the village of F. León, and extended for approximately 1 km downstream. A hot lake with a volume of $\sim 26 \times 10^6$ m^3 formed behind the dam in late April (Fig. 3.7), and increased up to $\sim 40 \times 10^6$ m^3 in early May, when total rainfall was estimated to be ~70 mm (Quintas 2000). It extended 4 km upstream to the confluence between the Magdalena and Susnubac rivers (Medina-Martínez 1982, Fig. 3.7). This dam failed by overtopping on May the 26th at 0130 UT. A hot flow, with temperatures of ~90 °C at Xochimilco and ~82 °C at Ostuacán, mixed with the waters of the Grijalva river, 28 km downstream, and traveled up to 35 km downstream reaching the Peñitas hydroelectric dam, which was in construction, killing 1 person and injuring other 3. Lahar deposits from the event of May 26th are exposed along the Platanar river as four flat terraces and cover a minimum area of 1.1×10^6 m^2 with an average thickness of 4 m (Macías et al. 2008). Only the Moba river, to the East, was unaffected by this dam failure.

In summary, ≈2.2 km^3 of trachyandesitic (56–57.5 wt% SiO_2) tephra, corresponding to 1.1 km^3 DRE at 2.6 g/cm^3 were erupted during the 1982 eruption (Carey and Sigurdsson 1986). No significant compositional or mineralogical differences were observed among the three fallout layers A1, B and C, characterized by a mineral association consisting of plagioclase (An_{32-80}) + hornblende + augite + apatite + biotite + anhydrite ± Ti-magnetite ± sphene and pyrrhotite (Luhr et al. 1984). Anhydrite crystals (up to 2 wt%) were recognized for the first time in fresh pumice from the eruption, occurring both as discrete phenocrysts and inclusions in other silicate crystals, indicating that they precipitated from a S-rich (2.6 wt% SO_3) melt (Luhr et al. 1984; Varekamp et al. 1984; Luhr and Logan 2002; Luhr 2008). This sulfur content, considered too large to have been dissolved in the melt at pre-eruptive magmatic temperatures of 800–850 °C (see Chap. 2), suggest that a significant fraction of the erupted S was present as a separate gas phase prior to eruption (Luhr et al. 1984). Part of this sulfur was inferred to be released as an oxidized vapor phase in the eruptive clouds (Varekamp et al. 1984), and absorbed into the ash after oxidation, determining premature fallout of particles of different grain-sizes and producing a polymodal distribution in ash fallout layers (Varekamp et al. 1984).

Nevertheless, the occurrence of different types of aggregates cemented by a film rich in sulfur, similar (i.e. internal grain-size distribution, sorting, and morphology) to sulfur aggregates described on the slopes of small sulfur cones, formed on the crater floor at Poás volcano when the lake dried out (Oppenheimer 1992), suggests that also at El Chichón liquid sulfur acted as a binder between particles (Scolamacchia and Dingwell 2014).

Liquid sulfur was eventually explosively ejected during most of the eruptive events, being more abundant in deposits produced at the onset of activity that caused the flashing of the hydrothermal system on April 3 at 0912 UT (S1-0), and in those produced shortly after the onset of the phreatoplinian activity C (S3-3). The abundance of cemented irregular clusters in deposits produced during the last phases of the eruption (i.e. unit S3) suggests that the supply of liquid sulfur was long lasting. Therefore, it is reasonable to think that native/elemental sulfur was probably slowly accumulated in the hydrothermal system at El Chichón, by precipitation from condensing magmatic components (i.e. SO_2 and H_2S), emitted from the degassing trachyandesitic magma, similar to what reported at other andesitic volcanoes with active hydrothermal systems, where vapor-dominated areas surrounded by brine solutions, characterize the hydrothermal systems (e.g. Bennet and Raccicchini 1978; Oppenheimer and Stevenson 1989; Oppenheimer 1992; Christenson and Woods 1993; Christenson 2000; Christenson et al. 2010).

Supporting this hypothesis, Mülleried (1933) described the presence of stalactites of native sulfur near fumaroles discharging H_2S almost 50 years before the 1982 eruption; similar features were also observed in ejecta from Poás (Bennet and Raccicchini 1978; Francis et al. 1980) and Ruapehu (Nairn et al. 1979), and interpreted as an evidence of the presence of liquid sulfur.

Between 5 and 9 million tons of SO_2 were emitted into the atmosphere during the 1982 eruption (Krueger et al. 1995), corresponding to a cumulative mass of 7.5 million tons, according to more recent estimates (Krueger et al. 2008). This amount was only exceeded by the eruption of Pinatubo in 1991. The massive injection of sulfur in the stratosphere caused a 5–6 °C warming in the tropical lower stratosphere, already in October 1982 (Parker and Brownscombe 1983).

3.3 Characteristic Activity and Hazard Assessment

The stratigraphic record for the El Chichón Volcanic Complex gives an idea of the most frequent kind of eruptions, as well as the approximate maximum distribution of related deposits.

Beside the frequent dome extrusions that occurred during the construction of the Somma edifice (see Sect. 3.2), accompanied in some cases by their explosive destruction, the stratigraphic record available for the Holocene, indicate that the eruptive activity was mostly explosive in character. Only two episodes of effusive activity are documented during the Holocene, and were apparently related to a subordinate activity associated to dome emplacement. The maximum run-out of lava flows was limited to the first 1–2 km from the present crater on the Somma flanks to the NE (unit M of Espíndola et al. 2000) and the W, associated to the pre-1982 dome (Fig. 3.2a).

According to past records, pyroclastic density currents generated by the collapse of eruptive columns of different altitudes seem to represent one of the most frequent eruptive phenomena. The deposits from such activity are generally confined to main ravines draining the volcano, flowing maximum distances of 4 km to the NW (at ~7,700 year BP), 3 km to the NE (~2,040 year BP, and ~900 year BP), and 4.3 km E (~2,400 and ~1,800 year BP). An exception is represented by the deposits dated at ~3,675 year BP, which were able to travel as far as 10 km to the E and S, according to Espíndola et al. (2000). The areal extent of this deposit suggests that this event was the greatest in magnitude of those that have occurred at El Chichón, but more detailed studies would be necessary to confirm this hypothesis.

Block and ash flows were produced by the explosive disruptions of central domes that grew inside the Somma crater, around 3,045 year BP, 1,500 year BP and during the last eruption. Stratigraphic records indicate that this kind of activity produced flows that were mainly confined in major ravines at distances between 2 (unit J), and 2.5 (unit E) km to the E. Their areal distribution resembles that of PF1 and PF2 produced during the 1982 eruption, which were partially confined by the Somma walls, and followed the path of major tributaries around the crater, reaching up to 4 km S and W, where they were blocked by the Susnubac and Magdalena rivers. Apparently, some of them were able to travel to the NW and NE along El Platanar Valley up to 4.5 km (**Unit E**).

The only possible evidence for eruptive activity involving the collapse of a plinian column is suggested by the presence of a fallout layer at the base of a pumice-rich deposit (Tilling et al. 1984). This event generated several pyroclastic density currents, which

were recognized up to 2.5 km to the East (~1,250 year BP, **Unit D**). The apparent lower extent of these deposits can be attributed to post-depositional erosion or to a lack of outcrops, due to subsequent burial from younger deposits.

According to the information available, the interaction between rising magma with external water (likely groundwater, see below) occurred at least five times in the last 10,000 years. The Guayabal tuff cone located on the flanks of Somma represents the first record of this kind of activity. The extension of deposits from this eruptive center cannot be determined as the edifice is only partly preserved. Possible evidence for hydromagmatic activity from the central crater exists for deposits dated around 3,100 (unit J), 1,900 year BP (unit G), 1,500 year BP (unit E), even if more detailed studies would be necessary to confirm the stratigraphic data, and numerous hydromagmatic events are well documented during the last eruption in 1982. During the 1,500 year BP eruption, and in 1982, this kind of activity accompanied dome destruction. The 1982 eruptive events were characterized by different water/magma ratios. This alternation of eruptive events was likely caused by the interaction of rising magma with a water table located at shallow depths. This hypothesis is consistent with the presence of springs located at different altitudes on the Somma flanks, observed before the 1982 eruption (Templos 1981; Casadevall et al. 1984), and the formation of a lake inside the crater within a few weeks from the 1982 eruption, interpreted as due to the inflow of groundwater (Casadevall et al. 1984). Recent studies on the origin of waters from the springs located on the W and SE flanks of the volcano (see Chap. 4), would confirm the presence of a widespread (ca. 3.5 km^2), shallower aquifer at depths of ~280 m beneath the crater, at the contact between the volcanic rocks and the sedimentary basement, beside a more deeper one, located at depths of ~2 km inside the Cretaceous basement.

In light of new data, the earlier hypothesis of the existence of a multiple conduit system, to explain the occurrence of phreatomagmatic activity contemporaneous to the collapse of the plinian column B (Scolamacchia and Macías 2005), now can be discarded. In fact, recent analyses of magnetic anomalies inside the crater formed in 1982 (Juetzler et al. 2011) ruled out the presence of a multiple conduit system beneath El Chichón.

The presence of fumaroles discharging H_2S, and hot springs described on the volcano flanks (Mülleried 1933; Templos 1981; Canul and Rocha 1981) suggested the presence of a hot water hydrothermal system overlain by a small vapor-dominated cap before the 1982 eruption (Casadevall et al. 1984; Rye et al. 1984). The flashing of this hydrothermal system eventually triggered one of the most energetic events, responsible for the destruction of a great portion of the dome on 3 April.

Hydrothermal fluids were involved in different amounts during several eruptive events together with liquid sulfur as attested by the presence of ash aggregates cemented by a film rich in S Fe, and minor P with variable amounts of Na, Mg, and Ca.

Eventually the binding action of liquid sulfur was particularly efficient in removing from the eruptive clouds not only particles in the size range of ash but also in the size of lapilli (>2 mm) as attested by the maximum dimensions of the fragments accreted (Scolamacchia 2014; Scolamacchia and Dingwell 2014). These dimensions exceed those (10–100 μm) commonly removed by water bridges or electrostatic attraction (e.g. Sheridan and Wohletz 1983b; Schumacher and Schmincke 1995; Brown et al. 2010, 2012).

Even if the hydrothermal system of the volcano was partially destroyed during the 1982 eruption, a new one was established shortly after as attested by the active hydrothermal areas present inside the crater (Casadevall et al, 1984; see Chap. 4). According to Juetztler et al. (2011), the main heat source for the present lake-spring hydrothermal system would be provided by the remnants of the dome destroyed in 1982, corresponding to high magnetic anomalies observed inside the 1982 crater in correspondence of active hydrothermal areas inside the present crater. Other thermal manifestations would be controlled by the upper portions of the hydrothermal system formed after the last eruption, as indicated by recent geochemical studies (Chap. 4).

The generation of lahars must have been frequent during El Chichón eruptive history, considering the high precipitation rate in the area (4,000 mm/year, Atlas del Agua 1976), and the abundance of unconsolidated volcaniclastic material. Lahar deposits were recognized intercalated to deposits of blocks and ash during the early stages of construction of the Somma edifice (see Sect. 3.2), and a precise record of events exists for the 1982 eruption, which deposits are

exposed along the Platanar river (see Sect. 3.2). Numerical simulations, using post-1982 topography, indicated that future lahars (1×10^6 m^3 in volume) could inundate villages along the Platanar and Magdalena rivers, and an extraordinary flooding event such as the 1982 lake break-out (3×10^6 m^3) could potentially reach the town of Ostuacan (12.5 km NW) along the Magdalena river, also affecting the Grijalva river system (Macias et al. 2008).

Pyroclastic fall deposits, from plinian eruptive column(s), were recognized only in 3 of the 12 explosive eruptions during the Holocene, corresponding to the 1,250 year BP (Unit D Tilling et al. 1984), the 550 year BP (unit B) and the 1982. The areal distribution of unit B was greater than the 1982 fall products, and dispersed ashes across an area of 240 km^2, according to the 20 cm isopach (Macías et al. 2003). Taking into account the prevailing wind directions during different seasons, directed to the E during spring, summer and autumn, more dispersed in all direction during winter, and the isopach of the most dispersed fallout layer of the 1982 eruption (A1), an area of 45,000 km^2 to the NE would be covered by a distal fallout 1 mm, if a similar event would occur in the future (Macias et al. 2008). Based on the numerical simulation of the 1982 plinian events and using daily wind records spanning the last 20 years (1991–2010), Bonasia et al. (2012) indicated that for a moderate eruption (e.g. fallout A1, VEI > 4), an area of 4,000 km^2 would have a probability greater than 2 % of being covered by a ash load exceeding 100 kg/m^2 (minimum value considered critical for structural damages). This probability would increase to more than 5 % for a VEI > 5 eruption (e.g. fallouts A1 + B +C), across an area of 12,000 km^2 including the city of Villahermosa, capital of Tabasco. This last scenario, would affect more than 1 million people and the air traffic in the area.

The most likely eruptive scenarios within a given time span was evaluated by Mendoza-Rosas and De la Cruz-Reyna (2010) using a probabilistic analysis considering Holocene and historical eruption time-series based on their magnitudes (VEI 2 to 5). Their study evaluated the probabilities of occurrence of at least one eruption exceeding a given VEI in a determined time interval (20, 50, 100 and 500 years). In these terms eruptions with a VEI > 4, such as the 29 March at 0532 UT and 4 April at 1122 UT during the 1982 eruption (Macías et al. 2008), would have a probability of 10 % in 100 years, and one of 39 % in 500 years, to occur. This second scenario would be confirmed by the 550 year BP plinian eruption. The most probable event with a VEI > of 2 or 3, calculated for a 500 years interval, would have probabilities of 74 and 57 % respectively to occur. A similar scenario was envisaged by Espindola et al. (2000), who used a statistical method to have a rough estimate of the eruption rate based on the ten repose periods of the past 3,700 years. This analysis yields a 22 % probability for an eruption similar to the 1982 within the next 100 years to occur (Espindola et al. 2000).

For hazard assessments, it is necessary to take into account that the main topographic irregularities related to the regional folds and fault system (García-Palomo et al. 2004), or ancient structures such as the Somma crater (Figs. 3.1 and 3.2a), because they can influence the courses, hence distribution, of different types of gravity-driven flows, in a radius between 1.5 and 2 km, and between 3.5 and 5 km from the crater.

The three notches that dissect the Somma crater to the E, N and SW, corresponding to the river source of El Platanar to the E, S. Pablo Cambac to the N and Tuspac to the S, represented main "pathways" for the initial dispersion of most of the pyroclastic density currents. The walls of this ancient crater were able to control the distribution of some PDCs (e.g. unit IU) to the SE where they are 1,100 m a.s.l. high, but not to the NE, where they reach only 900 m a.s.l. The best exposures of Holocene deposits, and the most complete sections of the last eruption, occur in the eastern sector, reflecting the smooth topography determined by the presence of the San Juan fault (García-Palomo et al. 2004), which favored a greater dispersion of most of the gravity driven flows to the E-SE (Sigurdsson et al. 1984; Espíndola et al. 2000; Scolamacchia and Macías 2005). Variations of a few degrees in the topographic gradient at ~2 km from the crater, contributed to destabilize most of the flows, as suggested by the structural features in the exposed PDCs deposits (i.e. units PF1 and S2, Macías et al. 1998; Scolamacchia and Macías 2005), indicating that the currents dropped their coarser load at this distance. Nevertheless, diluted PDCs continued to travel with high momentum for almost 3 km into the 2–2.5 km wide El Platanar plain, where the topography gently declined from 620 to 500 m a.s.l., destroying the village of Volcán Chichonal between 3.6 and 4.7 km E. It is noteworthy that a new settlement was established

there a few years ago, almost at the same distance (from the volcano summit) of site buried during the 1982 eruption.

Considering the areal distribution of the deposits of the 1982 eruption, it is reasonable to believe that diluted PDCs, with a low solids concentration, (i.e. pyroclastic surges, 0.1–1 vol%, Wilson and Houghton 2000), represent the most destructive phenomena, because they were poorly controlled by the topography and were able to reach greater distances with respect to other types of flows. The extension, textural and structural characters of the deposits and the eyewitness accounts of the 1982 eruption, indicate that some of these currents reached distances of 8.5 km to the S, 9.5 km NE and 10.5 km E, being able to down trees at distances of ~7 km to the E. All villages at a radial distance of 5 km from the crater were completed buried by the pyroclastic products of the eruption, but apparently these kinds of currents (i.e. base surges produced by magma-water interaction), caused the greater damages. Steel reinforced bars of house foundations embedded in these deposits, were observed bent in the same directions of the currents attesting their high dynamic pressure (Valentine 1998) at distances between 3.5 and 4 km (Scolamacchia and Schouwenaars 2009).

In the village of Esquípula Guayabal 3.5 km SE from the crater (Fig. 3.7), the impacts caused by ash particles hundreds of microns in size were found on a steel basketball pole remaining at its original position. Based on the deformation observed in the steel structure, a range of particle's velocities between 710 and 980 m/s were obtained (Scolamacchia and Schouwenaars 2009). Such velocities, much higher with respect to the speeds considered typical for pyroclastic density currents (tens to few hundreds m/s e.g. Druitt 1998; Wilson and Houghton 2000; Morrissey and Mastin 2000; Branney and Kokelaar 2002) are in the range of those observed for the initial air shocks produced during nuclear explosions (~1,000 m/s, Wohletz 1998; Valentine 1998), and those predicted theoretically and numerically for shock waves accompanying explosive eruptions (Wohletz et al. 1984; Wohletz and Valentine 1990). The impacts were attributed to an acceleration induced by shock waves, due to an efficient momentum coupling between a gas phase inside the clouds and the particles (max 280 μm in size) such that a sudden expansion of the gas caused by shock wave(s) was able to drag the particles up to high speeds (Scolamacchia and Schouwenaars 2009). Shock waves have been recorded and observed several times during explosive eruptions (e.g. Gorshkov 1959; Nairn 1976; Ishihara 1985), and their occurrence is to be expected in eruptions characterized by an unsteady discharge of material (Wohletz and Valentine 1990). Such conditions would occur during short-lived explosions (e.g. Vulcanian activity), the rapid decompression of a dome or cryptodome (e.g. Kieffer 1981a), the initial stages of caldera forming eruptions (Wohletz et al. 1984; Valentine and Wohletz 1989), or hydromagmatic eruptions, where shock waves generation has been experimentally observed and attributed to the heat energy transfer from magma to water during the fragmentation process (Zimanowski 1998).

The probability of atmospheric shock waves generation due to an unsteady discharge of material at the vent is realistic for the eruptive events occurred in 1982 at El Chichón (both during magmatic and phreatomagmatic phases of the eruption).

Moreover, when the reservoir pressures exceed atmospheric pressure by a factor of 5 (i.e. $P_{res/amb} > 5{:}1$, which are likely in explosive volcanic eruptions, a secondary system of shocks may form within the discharging supersonic eruptive plume, almost immediately after the passage of the flow head ("underexpanded jet" of Kieffer 1981a, b; Kieffer and Sturtevant 1984).

Such complex system of secondary shocks, consisting of crossed oblique shocks, and a perpendicular Mach disk shock, may propagate at distance of several vent diameters, reaching a steady location before collapsing back when the pressure of the reservoir decreases to sonic values. Recent scaled experiments and numerical simulations (Orescanin et al. 2010) indicated that in unsteady eruptive events (e.g. Vulcanian and blast-type), a Mach disk shock could generate at the vent, and propagate downstream until reaching equilibrium distances that, for $P_{res/amb}$ 150:1, can be in the order of 240 m from the vent, for vulcanian events resembling those occurred at Soufrière Hills volcano in 1997, and up to 7 km for a blast-type event such the one occurred at Mount St Helens in 1980. For a blast-type event with ratios $P_{res/amb}$ between 100:1 and 250:1, such distances would vary between 5.7 and 9 km, and the Mach disk would remain at its equilibrium location, for periods between 84 and 104 s before collapsing back toward the vent (Orescanin et al. 2010).

In this light, the distance from the crater at which the basketball pole impacted by ash was found (3.5 km) it is not unrealistic and the establishment of Mach disk shock structure, could have likely occurred also during the 1982 eruption of El Chichón.

In any of these scenarios the occurrence of such phenomena would have important implications for hazard assessments, but is not taken into account (Scolamacchia and Schouwenaars 2009).

3.4 Appraisal of the Eruptive History of El Chichón Volcano

By combining previous studies with unpublished K–Ar and $^{40}Ar/^{39}Ar$ dating on newly mapped stratigraphic units it was now possible to delineate a more complete scenario of the volcanic activity in time and space at El Chichón.

This recent information contributes to fill in the temporal gaps in the reconstruction of the eruptive history of the volcano, indicating that volcanic activity in the area was long-lasting, and occurred from several eruptive centers, controlled by a regional system of conjugated dextral strike-slip N-S, and a sinistral strike slip E-W faults.

Volcanism at El Chichon began around 1.64 My on the trace of a major NNW-SSE fault (the recently mapped Chichón–Catedral fault), building a major edifice, Catedral volcano, which later collapsed to the SE. The volcanism migrated 14 km to the SE around 1 My at the eastern tip of the E-W strike-slip San Juan fault with the emplacement of a trachybasaltic dike. The onset of activity at its present position began apparently already around 372 ka, according to $^{40}Ar/^{39}Ar$ ages obtained on a lava fragment from 1982 pyroclastic deposit, but no field evidence of this activity has been found until now. The construction of the Somma edifice was characterized by frequent extrusions of domes since about 276 ka. A major eruption destroyed the central part of the Somma dome complex apparently during late Pleistocene, forming a 1.5 km wide crater. According to new data, dome-building activity was contemporary to the Somma edification, resulting in the construction of the SW dome around 217 ka, the Cambac dome, on the NW sector, around 187–168 ka, and the Capulin domes, on the NNE, around 152 ka. Both Cambac and Capulin domes were subsequently explosively destroyed with the formation of block and ash flows, and following lahars, which are widely dispersed on the Somma flanks. During this explosive activity, another dome was extruded to the NW flank of the Somma, about 97–80 ka.

Explosive activity, mostly hydromagmatic in character built the Guayabal cone on the SE Somma flanks, on the trace of the major Chichón-Catedral fault, around 10 ka. This poorly preserved structure, collapsed toward the SE, was apparently active also during the Holocene.

The eruptive activity during the Holocene has been almost exclusively explosive in character, occurring from the same vent that was reactivated in 1982. Even with no substantial changes in the composition of the products, which have been always trachyandesitic, periods of dome growth followed by their explosive disruption alternated with eruption under open crater conditions, during which the interaction between magma and external water occurred at least five times. The stratigraphic record of the last 4,000 years, including the 1982 eruption, suggests a recurrence interval from a minimum of 100 years to a maximum of 600 years.

A better definition in time of the different phases of the 1982 eruption, was possible thanks to the analysis of the records from far away stations and eyewitnesses accounts that were not analyzed in previous works. Such interpretation is more consistent with the existing data, suggesting that the most destructive events, with the generation of PDCs, had already occurred by the early morning of 3 April (after 0312, local time), instead of on 4 April at 0139 UT as reported in previous eruption chronologies (i.e. Sigurdsson et al. 1984 and following studies). At this time, in fact, all existing records point toward the generation of the second Plinian event B.

The occurrence of aggregates cemented by a sulfur-rich film unevenly distributed among wet surge deposits of the 1982 eruption, being more abundant in those produced at the beginning of the events occurred on April 3, and after the phreatoplinian eruption on April 4, suggest that liquid sulfur was explosively ejected during several eruptive phases. Therefore it is likely that the accumulation of sulfur layers occurred also at El Chichón, as observed at other volcanoes with active hydrothermal systems. Considering the maximum sizes of individual fragments accreted (>2 mm), and the distribution of cemented aggregates,

the binding action of such substance was able to remove coarser particles, in the size of lapilli from eruptive clouds already at distances of few km from the vent.

Such evidences have important implications on the volumetric estimates of different grain sizes inside eruptive clouds, and should be considered in models of particles dispersion and sedimentation from eruptive plumes.

No dome began to grow after the 1982 eruption, and the absence of a large positive magnetic anomaly inside the newly formed crater suggests that it will not likely grow any time soon in the near future. Nevertheless, the precipitation of elemental sulfur, and other alteration minerals, from acid solutions generated by condensing volatiles exsolved from andesitic magma bodies, has been invoked to reduce rock permeability. Such process should be critically considered for its possible role in sealing the active hydrothermal system, determining its overpressurization, and leading to phreatic eruptions. In addition, due to the presence of a shallow groundwater table, also the probability of phreatomagmatic eruptions should be taken into account.

References

Albarrán J (1983) Experiencias de campo y reseña de la actividad del volcán Chichonal en Abril de 1982. In: IdG UNAM (ed) El volcán Chichonal VI Convención Geologica Nacional- Sociedad Geologica Mexicana. UNAM, Mexico DF, Mexico, pp 57–67

Austin-Erickson A, Büttner R, Dellino P, Ort MH, Zimanowski B (2008) Phreatomagmatic explosions of rhyolite magma: experimental and field evidence. J Geophys Res 113: B11201. doi:10.1029/2008JB005731

Atlas del Agua de la República Mexicana (1976) Secretaría de Recursos Hidráulicos, México, 253 pp

Belousov A, Voight B, Belousova M (2007) Directed blasts and blasts-generated pyroclastic density currents: a comparison of the Bezymianni 1956, Mount St Helens 1980, and Soufriére Hills, Monteserrat 1997 eruptions and deposits. Bull Volcanol 69(7):701–740

Bennet FD, Raccicchini SM (1978) Subaqueous sulphur lake in Volcan Poas. Nature 271:342–344

Branney MJ, Kokelaar BP (2002) Pyroclastic density currents and the sedimentation of ignimbrites. Geol Soc Lond Mem 27:143

Brinkley SRJ, Kirkwood JG, Lapson CW, Revelle R, Smith AL (1950) Shock from underwater and underground blasts. In: Los Alamos Scientific Laboratory: the effects of atomic weapons. U. S. Printing Office, Los Alamos, New Mexico, pp 83–113

Brown RJ, Branney MJ, Maher C, Dávila-Harris P (2010) Origin of accretionary lapilli within ground-hugging density currents: evidence from pyroclastic couplets on Tenerife. Geol Soc Am Bull 122(1/2):305–320

Brown RJ, Bonadonna C, Durant AJ (2012) A review of volcanic ash aggregation. Phys Chem Earth, Part A/B/C 45–46:65–78

Bonasia R, Costa A, Folch A, Macedonio G, Capra L (2012) Numerical simulation of tephra transport and deposition of the 1982 El Chichón eruption and implications for hazard assessment. J Volcanol Geotherm Res 231–232:39–49

Büttner R, Zimanowski B (1998) Physics of thermo-hydraulic explosions. Phys Rev E 57:5726–5729

Büttner R, Dellino P, Zimanowski B (1999) Identifying magma-water interaction from the surface features of ash particles. Nature 401:688–690

Bursik M (2001) Effect of wind on the rise height of volcanic plumes. Geophys Res Lett 18:3621–3624

Canul RF, Rocha VL (1981) Informe geológico de la zona geotérmica de "El Chichonal". Chiapas Comisión Federal de Electricidad, Morelia, México. Informe 32–81:38

Canul RF, Razo AM, Rocha VL (1983) Geología e historia volcanológica del volcán Chichónal, Estado de Chiapas. Revista del Instituto de Geología, U.N.A.M., México, pp 3–22

Carey S, Sigurdsson H (1986) The 1982 eruption of El Chichón volcano, Mexico (2): observation and numerical modelling of tephra-fall distribution. Bull Volcanol 48:127–141

Carey S, Sigurdsson H (1989) The intensity of Plinian eruptions. Bull Volcanol 51:28–40

Cas RAF, Wright JV (1987) Volcanic successions: modern and ancient. Chapman & Hall, London, 528 pp

Casadevall TJ, De la Cruz-Reyna S, Rose WI, Bagley S, Finnegan DL, Zoller WH (1984) Crater lake and post-eruption hydrothermal activity, El Chichón Volcano, Mexico. J Volcanol Geotherm Res 23:169–191

Christenson BW (2000) Geochemistry of fluids associated with the 1995–1996 eruption of Mt. Ruapehu, New Zealand: signatures and processes in the magmatic-hydrothermal system. J Volcanol Geotherm Res 2000:1–30

Christenson BW, Wood CP (1993) Evolution of a vent-hosted hydrothermal system beneath Ruapehu Crater Lake, New Zealand. Bull Volcanol 55:547–565

Christenson BW, Reyes AG, Young R, Moebis A, Sherburn S, Cole-Baker J, Britten K (2010) Cyclic processes and factors leading to phreatic eruption events: insights from the 25 September 2007 eruption through Ruapehu Crater Lake, New Zealand. J Volcanol Geotherm Res 191:15–32

Colgate SA, Sigurgeisson T (1973) Dynamic mixing of water and lava. Nature 244:552–555

Cole PD, Guest JE, Duncan AM, Pacheco JM (2001) Capelinhos 1957–1958, Faial Azores: deposits formed by an emergent surtseyan eruption. Bull Volcanol 63:204–220

Costa A, Macedonio G, Folch A (2006) A three-dimensional Eulerian model for transport and deposition of volcanic ashes. Earth Plan Sci Lett 241:634–647

Damon P, Montesinos E (1978) Late Cenozoic volcanism and metallogenesis over an active Benioff zone in Chiapas, Mexico. Ariz Geol Soc Dig XI:155–168

De la Cruz Reyna S, Martin Del Pozzo AL (2009) The 1982 eruption of El Chichón volcano, Mexico: eyewitness of the disaster. Geofis Int 48:21–31

Druitt TH (1998) Pyroclastic density currents. In: Gilbert JS, Sparks RSJ (eds) The physics of explosive volcanic eruptions. Geological Society of London, Special Publication, London, pp 145–182

Duffield W, Tilling R, Canul RF (1984) Geology of El Chichón volcano, Chiapas, Mexico. J Volcanol Geotherm Res 20:117–132

Espíndola JM, Macías JL, Tilling R, Sheridan MF (2000) Volcanic history of El Chichón volcano (Chiapas, Mexico) during the Holocene and its impact on human activity. Bull Volcanol 62:90–104

Fisher RV (1990) Transport and deposition of pyroclastic surge across an area of high relief: the 1980 eruption of Mount St. Helens, Washington. Geol Soc Am Bull 102:1038–1054

Fisher RV, Waters A (1970) Base surge bed forms in maar volcanoes. Am J Sci 268:157–180

Fisher RV, Schmincke, HU (1984) Pyroclastic rocks. Springer, Berlin, 472 pp

Folch A, Costa A, Macedonio G (2009) FALL3D: a computational model for transport and deposition of volcanic ash. Comput Geosci 35(6):1334–1342

Francis PW, Thorpe RS, Brown GC, Glasscock J (1980) Pyroclastic sulphur eruption at Poás volcano, Costa Rica. Nature 283:754–756

Freundt A, Bursik M (1998) Pyroclastic flow transport mechanisms. In: Freundt A, Rosi M (eds) From magma to tephra. Elsevier, Amsterdam, pp 173–231

García-Palomo A, Macías JL, Espíndola JM (2004) Strike-slip faults and K-alkaline volcanism at El Chichón volcano, southeastern Mexico. J Volcanol Geotherm Res 136:247–268

Gorshkov GS (1959) Gigantic eruption of the Volcano Bezymianny. Bull Volcanol 20:77–109

Gorshkov GS (1963) Directed volcanic blasts. Bull Volcanol 26:83–88

Heiken GH (1971) Tuff rings: examples from the Fort Rock - Christmas Lake Valley basin, south-central Oregon. J Geophys Phys Res 76:5615–5626

Haskov J, De la Cruz Reyna S, Sing SK, Medina F, Gutiérrez C (1983) Seismic activity related to the March–April 1982 eruption of El Chichón volcano, Chiapas, Mexico. Geophys Res Lett 10(4):239–296

Heiken GH, Wholetz K (1985) Volcanic ash. University of California Press, Berkeley, p 246

Hoblitt R, Miller CD, Wallance JW (1981) Origin and stratigraphy of the deposit produced by the May 18 directed blast. In: Lipmann PW, Mullineaux DR (eds) The 1980 eruption of Mount St. Helens, Washington. Washington D. C., pp 401–419

Hoblitt RP, Wolfe EW, Scott WE, Couchman MR, Pallister JS, Javier D (1996) The Preclimactic eruptions of Mount Pinatubo, June 1991. In: Newhall CG, Punongbayan, RS (eds) Fire and mud. University of Washington Press, Washington D.C., pp 457–511

Ishihara K (1985) Dynamic analysis of volcanic explosions. J Geodyn 3:327–349

Jimenez Z, Espíndola VH, Espíndola JM (1999) Evolution of the seismic activity from the 1982 eruption of El Chichón Volcano, Chiapas, Mexico. Bull Volcanol 61:411–422

Jutzeler M, Varley N, Roach M (2011) Geophysical characterization of hydrothermal system and intrusive bodies, El Chichón volcano (Mexico). J Geophys Res 116:B04104

Kieffer SW (1981a) Blast dynamics at Mount St. Helens on 18 May 1980. Nature 291:568–570

Kieffer S (1981b) Fluid dynamics of the May 18 blast at Mount St. Helens. In: Lipman PW, Mullineaux, DR (eds) The 1980 eruptions of Mount St. Helens, Washington. U.S. Geological Survey, pp 379–400

Kieffer S, Sturtevant B (1984) Laboratory studies of volcanic jets. J Geophys Res 89:8253–8268

Kokelaar BP (1986) Magma-water interaction in subaqueous and emergent basaltic volcanism. Bull Volcanol 48:275–289

Krueger A (1983) Sighting of El Chichón sulfur dioxide clouds with the Nimbus 7 Total Ozone Mapping Specrometer. Science 220(4604):1377–1379

Krueger AJ, Walter LS, Bhartia PK, Schnetzler CC, Krotkov NA, Sprod I, Bluth GJS (1995) Volcanic sulfur dioxide measurements from the total ozone mass spectrometer instruments. J Geophys Res 100:14057–14076

Krueger A, Krotov N, Carn S (2008) El Chichon: the genesis of volcanic sulfur dioxide monitoring from space. J Volcanol Geotherm Res 175:408–414

Layer PW, García-Palomo A, Jones D, Macías JL, Arce JL, Mora JC (2009) El Chichón volcanic complex, Chiapas, México: stages of evolution based on field mapping and $^{40}Ar/^{39}Ar$ geochronology. Geofís Int 48:33–54

Lorenz V (1974) Vesiculated tuffs and associated features. Sedimentology 21:273–291

Luhr JF (2008) Primary igneous anhydrite: progress since its recognition in the 1982 El Chichón trachyandesite. J Volcanol Geotherm Res 175:394–407

Luhr JF, Logan MAV (2002) Sulfur isotope systematics of the 1982 El Chichón trachyandesite: a ion micropobe study. Geochim Cosmochim Acta 66(18):3303–3316

Luhr JF, Carmichael ISE, Varekamp JC (1984) The 1982 eruption of El Chichón volcano, Chiapas, Mexico: mineralogy and petrology of the anhydrite bearing pumices. J Volcanol Geotherm Res 23:69–108

Macías JL (1994) Violent short-lived eruptions from small-size volcanoes: El Chichón, Mexico (1982) and Shtyubel, Russia (1907). Ph.D. dissertation, State University of New York, Buffalo

Macías JL, Sheridan MF, Espíndola JM (1997) Reappraisal of the 1982 eruption of El Chichón volcano, Chiapas, Mexico: new data from proximal deposits. Bull Volcanol 58:459–471

Macías JL, Espíndola JM, Bursik M, Sheridan MF (1998) Development of lithic-breccias in the 1982 pyroclastic flow deposits of El Chichón Volcano, Mexico. J Volcanol Geothermal Res 83:173–196

Macías JL, Arce JL, Mora JC, Espíndola JM, Saucedo R, Manetti P (2003) A 500-year-old Plinian eruption at El Chichón volcano, Chiapas, Mexico: explosive volcanism linked to reheating of the magma reservoir. J Geophys Res 108(B12):2569 doi:10.1029/2003JB002551

Macías JL, Capra L, Scott KM, Espíndola JM, García-Palomo A, Costa JE (2004) The 26 May 1982 breakout flows derived from a failure of a volcanic dam at El Chichón, Chiapas, Mexico. Geol Soc Am Bull 116(1–2):233–246

Macías JL, Capra L, Arce JL, Espíndola JM, García-Palomo A, Sheridan MF (2008) Hazard map of El Chichón volcano,

Mexico: Constraints posed by eruptive history and computer simulations. J Volcanol Geotherm Res 175(4):444–458
Macías JL, Arce JL, Garduño-Monroy VH, Rouwet D, Taran Y, Layer P, Jiménez A, Álvarez R (2010): Estudio de prospección geotérmica para evaluar el potencial del volcán Chichonal, Chiapas. Unpublished Report no. 9400047770 IGF-UNAM-CFE
Matson M (1984) The 1982 El Chichón volcano eruption-a satellite perspective. J Volcanol Geotherm Res 23:1–10
Mauk FJ (1983) Utilization of seismically recorded infrasonic acoustic signals to monitor volcanic explosions: the El Chichón sequence 1982- a case study. J Geophys Res 88:10385–310401
Medina-Martínez F (1982) El Volcán Chichón. GEOS 2(4):19
Mendoza-Rosas AT, De la Cruz-Reyna S (2010) Hazard estimates for El Chichón volcano, Chiapas, Mexico: a statistical approach for complex eruptive histories. Nat Haz Earth Syst Sci 10:1159–1170
Moore JC, Nakamura K, Alcaraz A (1966) The 1965 eruption of Taal volcano. Science 151:955–960
Moore JC (1967) Base surges in recent volcanic eruptions. Bull Volcanol 30:337–363
Moore JG, Sisson TW (1981) Deposits and effects of the May 18 pyroclastic surge. In: Lipmann PW, Mullineaux DR (eds) The 1980 eruptions of Mount St. Helens, Washington. Washington D.C., pp 421–438
Mooser F, Meyer-Abich, H, Mc Birney AR (1958) Catalogue of the active volcanoes of the world including Solfatara fields. Part VI, Central America. International Volcanological Association, Napoli, pp 26–30
Morrisey MM, Mastin L (2000) Vulcanian eruptions In: Sigurdsson H, Houghton B, Rymer H, Stix J, Mc Nutt S (eds) Encyclopedia of volcanoes. Academic Press, New York, pp 463–475
Mülliered FKG (1932) Der Chichón, ein bischer unbegannter tätiger Vulkan im nordlichen Chiapas, Mexiko. Zeit Vulkanol XIV:191–209
Mülliered F (1933) "El Volcán", único volcán en actividad descubierto en el estado de Chiapas. Mem Rev Acad Ciencias "Antonio Alzate" 54(11/12):411–416
Nairn IA (1976) Atmospheric shock waves and condensation clouds from Ngauruhoe explosive eruptions. Nature 259:190–192
Nairn IA, Wood CP, Hewson CAY (1979) Phreatic eruptions of Ruapehu: April 1975. NZ J Volcanol Geophys 22(2):155–173
Oppenheimer C (1992) Sulphur eruptions at Volcán Poás, Costa Rica. J Volcanol Geotherm Res 49:1–21
Oppenheimer C, Stevenson D (1989) Liquid sulphur lakes at Poás volcano. Nature 342:790–793
Orescanin MM, Austin JM, Kieffer SW (2010) Unsteady high-pressure flow experiments with application to explosive volcanic eruptions. J Geophys Res 115:B06206
Parker DE, Brownscombe JL (1983) Stratospheric warming following the El Chichón volcanic eruption. Nature 301:406–408
Quintas I (2000) Eric II. Documento de la base de datos climatológica y del programa extractor. Instituto Mexicano de Tecnología del Agua. Morelos, Mexico, 75 pp
Reimer PJ, Baillie MGL, Bard E, Bayliss A, Beck JW, Bertrand CJH, Blackwell PG, Buck CE, Burr GS, Cutler KB, Damon PE, Edwards RL, Fairbanks RG, Friedrich M, Guilderson TP, Hogg AG, Hughen KA, Kromer B, McCormac FG, Manning SW, Ramsey CB, Reimer RW, Remmele S, Southon JR, Stuiver M, Talamo S, Taylor FW, van der Plicht J, Weyhenmeyer CE (2004) IntCal04 Terrestrial radiocarbon age calibration, 26–0 ka BP. Radiocarbon 46:1029–1058
Richards AF (1959) Geology of the Islas Revillagigedo, Mexico. 1. Birth and development of Volcán Bárcena, Isla San Benedicto. Bull Volcanol 22:73–123
Rye RO, Luhr JF, Wasserman MD (1984) Sulfur and oxygen isotopic systematics of the 1982 eruptions of El Chichón volcano, Chiapas, Mexico. J Volcanol Geotherm Res 23:109–123
Rose WI, Bornhorst TJ, Halsor SP, Capaul WA, Plumey PS, De la Cruz Reyna S, Mena M, Mota R (1984) Volcán El Chichón, Mexico: pre S-rich eruptive activity. J Volcanol Geotherm Res 23:147–167
Scolamacchia T, Macías JL (2005) Distribution and stratigraphy of deposits produced by diluted pyroclastic density currents of the 1982 eruption of El Chichón volcano, Chiapas, Mexico. Rev Mex Cienc Geol 22:159–180
Scolamacchia T, Macías JL, Sheridan MF, Hughes SR (2005) Morphology of ash aggregates from wet pyroclastic surges of the 1982 eruption of El Chichón volcano, Mexico. Bull Volcanol 68:171–200
Scolamacchia T, Schouwenaars R (2009) High-speed impacts by ash particles in the 1982 eruption of El Chichón (Mexico). J Geophys Res 114:B12206
Scolamacchia T. (2012) "El Chichón 1982: reinterpretación de la cronología de los eventos eruptivos". Unión Geofísica Mexicana (UGM) General Meeting, Puerto Vallarta, México, October 28–November 2, 2012. Puerto Vallarta, Jalisco, Mexico
Scolamacchia T (2014) Another look to the mechanisms of formation of ash aggregates in pyroclastic deposits. In: Rocha R, Pais, J, Kullberg, JC, Finney S (eds) At the cutting edge of Stratigraphy. STRATI First International Congress on Stratigraphy, Lisboa, Portugal, 1–7 July 2013. Springer Geology, vol XLV. 1343 pp
Scolamacchia T, Dingwell DB (2014) Sulfur as a binding agent of aggregates in explosive eruptions. Bull Volcanol 76 (10):871. doi:10.1007/s00445-014-0871-1
Schumacher R, Schmincke HU (1995) Models for the origin of accretionary lapilli. Bull Volcanol 56:626–639
SEAN Smithsonian Institution (1989) Global volcanism 1975–1985. Prentice Hall, Englewood Cliffs, p 657
Sheridan MF, Wohletz K (1981) Hydrovolcanic explosions: the systematics of water-pyroclast equilibration. Science 212:1387–1389
Sheridan MF, Wohletz KH (1983a) Hydrovolcanism: basic considerations and review. J Volcanol Geotherm Res 17:1–29
Sheridan MF, Wohletz, KH. (1983b) Origin of accretionary lapilli from the Pompeii and Avellino deposits of Vesuvius. In: Gooley R (ed) Microbeam analysis. San Francisco Press, Phoenix, p 336
Sigurdsson H, Carey SN, Espíndola JM (1984) The 1982 eruption of El Chichón volcano, Mexico: stratigraphy of pyroclastic deposits. J Volcanol Geotherm Res 23:11–37
Sigurdsson H, Carey SN, Fisher RV (1987) The 1982 eruptions of El Chichón volcano, Mexico (3): physical properties of pyroclastic surges. Bull Volcanol 49(2):467–488

Sohn YK, Chough SK (1992) The Ilchulbong tuff cone, Cheju Island, South Korea: depositional processes and evolution of an emergent, Surtseyan-type tuff cone. Sedimentology 39:523–544

Sohn YK, Cronin SJ, Brenna M, Smith IEM, Németh K, White JDL, Murtagh RM, Jeon YM, Kwon CW (2012) Ilchulbong tuff cone, Jeju Island, Korea, revisited: a compound monogenetic volcano involving multiple magma pulses, shifting vents, and discrete eruptive phases. Geol Soc Am Bull 124 (3/4):259–274. doi:10.1130/B30447.1

Stuiver M, Reimer PJ (1986) A computer program for radiocarbon age calibration. Radiocarbon 28:1022–1030

Sulpizio R, Zanella E, Macías JL (2008) Deposition temperature of some PDC deposits from the 1982 reuption of El Chichón volcano (Chiapas, Mexico) inferred from rock magnetic data. J Volcanol Geotherm Res 175(4):494–500

Tahira M, Nomura M, Sawada Y, Kosuke K (1996) Infrasonic and acoustic-gravity waves generated by the Mount Pinatubo eruption of June, 15, 1991. In: Newhall CG, Punongbayan RS (eds) Fire and mud. University of Washington Press, Washington D.C., pp 601–612

Taylor GA (1958) The 1958 eruption of Mount Lamington, Papua. Austr Bur Min Resour Geol Geophys Bull 38:1–117

Templos LA, Munguia Bracamontes F, Barrera VM (1981) Observaciones geoquímicas en la zona geotérmica del Chichonál, Chiapas, Mexico. Unpublished report. Comisión Federal de Electricidad, Mexico. Informe 33–81:32

Tilling RI (2009) El Chichón "surprise" eruption in 1982: lessons for reducing volcano risk. Geofís Int 48(1):3–19

Tilling R, Rubin M, Sigurdsson H, Carey S, Duffield W, Rose WI (1984) Holocene eruptive activity of El Chichón volcano, Chiapas, Mexico. Science 224:747–749

Valentine GA (1998) Damage to structures by pyroclastic flows and surges, inferred from nuclear weapons effects. J Volcanol Geotherm Res 87:117–140

Valentine G, Wohletz KH (1989) Numerical models of Plinian eruption columns and pyroclastic flows. J Geophys Res 94:1867–1887

Valentine GA, Fisher RV (2000) Pyroclastic surges and blasts In: Sigurdsson H, Houghton B, McNutt SR, Hazel R, Stix J (eds) Encyclopedia of volcanoes. Academic Press, New York, pp 571–580

Varekamp JC, Luhr JF, Prestegaard KL (1984) The 1982 eruption of El Chichón volcano (Chiapas, Mexico): character of the eruptions, ash-fall deposits and gas phase. J Volcanol Geotherm Res 23:39–68

Walker GPL (1971) Grain-size characteristics of pyroclastic deposits. J Geol 79:696–714

Walker GL (1984) Characteristics of dune-bedded pyroclastic surge bedset. J Volcanol Geoth Res 20:281–296

Waters AC, Fisher RV (1971) Base surges and their deposits: Capelinhos and Taal volcanoes. J Geophys Res 76:5596–5614

White JDL (1991) Maar-diatreme phreatomagmatism at Hopi Buttes, Navajo Nation (Arizona), USA. Bull Volcanol 53:239–258

Widmer R, Zürn W (1992) Bichromatic excitation of long-period Rayleigh and air waves by the Mount Pinatubo and El Chichón volcanic eruptions. Geophys Res Lett 19(8):765–768

Wilson CJN, Houghton BF (2000) Pyroclastic transport and deposition In: Sigurdsson H, Houghton B, McNutt SR, Hazel R, Stix J (eds) Encyclopedia of Volcanoes. Academic Press, New York, pp 545–55

Wohletz KH (1983) Mechanisms of hydrovolcanic pyroclast formation: grain-size, scanning electron microscopy, and experimental studies. J Volcanol Geotherm Res 17:31–64

Wohletz KH, Sheridan MF (1979) A model for pyroclastic surge. Geol Soc Am Spec Pap 180:305–318

Wohletz KH, Sheridan MF (1983) Hydrovolcanic explosions II. Evolution of basaltic tuff rings and tuff cones. Am J Sci 283:385–413

Wohletz KH, Valentine GA (1990) Computer simulations of explosive volcanic eruptions. In: Ryan MP (ed) Magma transport and storage. Wiley, New York, pp 113–135

Wohletz KH, McGetchin TR, Sanford MT II, Jones EM (1984) Hydrodynamics aspects of caldera-forming eruptions: numerical models. J Geophys Res 89:8269–8285

Young GA (1965) The physics of base surge. In: U.S. Naval Ordenance Lab NOLTR 64-103, AD-618733, Wake Oak, Maryland, p 294

Zimanowski B (1998) Phreatomagmatic explosions. In: Freundt A, Rosi M (eds) From magma to tephra: modelling physical processes of explosive volcanic eruptions Elsevier Science Publications, Amsterdam, pp 25–54

Zimanowski B, Wohletz KH (2000) Physics of phreatomagmatism-I. Terra Nostra 6:515–523

Zimanowski B, Frölich G, Lorenz V (1991) Quantitative experiments on phreatomagmatic explosions. J Volcanol Geotherm Res 48:341–358

Zimanowski B, Büttner, R, Lorenz V (1997a) Premixing of magma and water in MFCI experiments. Bull Volcanol 58:491–495

Zimanowski B, Büttner R, Lorenz V, Häfele H G (1997b) Fragmentation of basaltic melt in the course of explosive volcanism. J Geophys Res 102(B1):803–814

Zürn W, Widmer R (1996) Worldwide observation of bichromatic long-period Rayleigh waves excited during the June, 15, 1991, eruption of Mount Pinatubo. In: Newhall CG, Punongbayan RS (eds) Fire and mud. University of Washington, Press Seattle, pp 615–624